

# Models for Metal-Poor Stars with Different Initial Abundances of C, N, O, Mg, and Si. II. Application to the Colour-Magnitude Diagrams of the Globular Clusters 47 Tuc, NGC 6362, M 5, M 3, M 55, and M 92

Don A. Vandenberg,<sup>1\*</sup> Luca Casagrande,<sup>2</sup> and Bengt Edvardsson,<sup>3</sup>

<sup>1</sup>*Department of Physics and Astronomy, University of Victoria, P.O. Box 1700, STN CSC, Victoria, BC, Canada V8W 2Y2*

<sup>2</sup>*Research School of Astronomy and Astrophysics, Mount Stromlo Observatory, The Australian National University, Canberra, A.C.T. 2611, Australia*

<sup>3</sup>*Theoretical Astrophysics, Department of Physics & Astronomy, Uppsala University, Box 516, SE-751 20 Uppsala, Sweden*

Accepted XXX. Received YYY; in original form ZZZ

## ABSTRACT

Stellar models for  $-2.5 \leq [\text{Fe}/\text{H}] \leq -0.5$  that have been computed for variations in the C:N:O abundance ratio (for two different values of [CNO/Fe]) are compared with *HST* Wide Field Camera 3 (WFC3) observations of the globular clusters (GCs) 47 Tuc, NGC 6362, M 5, M 3, M 55, and M 92. The BCs used to transpose the models to the observed planes are based on new MARCS synthetic spectra that incorporate improved treatments of molecules that involve atoms of C, N, and O. On the assumption of well-supported distance moduli and reddenings, isochrones for [O/Fe] = 0.6 and [m/Fe] = 0.4 for the other  $\alpha$  elements, which are favoured by binary stars in GCs, generally reproduce the main features of observed colour-magnitude diagrams (CMDs) to within  $\sim 0.03$  mag. In particular, they appear to match the spreads in the observed  $(M_{F336W} - M_{F438W})_0$  colours that are spanned by CN-weak and CN-strong stars along the lower giant branch quite well, but not the bluest giants, which are suspected to be N-poor ([N/Fe]  $\lesssim -0.5$ ). Both the absolute  $(M_{F438W} - M_{F606W})_0$  colours and the variations in these colours at a given  $M_{F606W}$  magnitude on the giant branch are difficult to explain unless the reddest stars are C-rich ([C/Fe]  $\gtrsim +0.5$ ). Allowing for moderate He abundance variations ( $\delta Y \sim 0.05$ ) improves the fits to the observations.

**Key words:** globular clusters – stars: abundances – stars: binaries – stars: evolution – stars: Population II – Hertzsprung-Russell and colour-magnitude diagrams

## 1 INTRODUCTION

Globular clusters (GCs) are known to contain multiple, chemically distinct, stellar populations. This has been established by the vast amount of spectroscopic work that has been carried out during the past 50+ years (see, e.g., the reviews by Freeman & Norris 1981, Smith 1987, Kraft 1994, Gratton et al. 2004), and by numerous photometric surveys since 2004 (e.g., Bedin et al. 2004, Piotto et al. 2007, Milone et al. 2010, Bellini et al. 2010). Chemical abundance studies have shown that O–Na and Mg–Al anticorrelations are typically found in GCs (Carretta et al. 2009b, and references therein), along with the ubiquitous variations of CN (e.g., Smith & Norris 1993, Grundahl et al. 1998, Briley et al. 2004, Cohen et al. 2005). Statistically significant Al–Si correlations have also been detected in a few clusters (Yong et al. 2005, Carretta et al. 2009b), as well as star-to-star variations of the iso-

topic ratios of Mg (Shetrone 1996, Yong et al. 2006). All of these findings can be explained by *p*-capture processes, provided that the temperatures in the nucleosynthesis site can reach sufficiently high values ( $\gtrsim 7 \times 10^7$  K in order for the Mg–Al cycle to operate).

Photometry has the important advantages over spectroscopy in giving one the capability to obtain observations of tens of thousands of stars simultaneously and to reach very faint luminosities. In recent years, multi-wavelength investigations have produced stunning colour-magnitude diagrams (CMDs) for many GCs, consisting of separate sequences of stars that can sometimes be distinguished all of the way from near the bottom of the main sequence (MS) to the upper red-giant branch (RGB); see, e.g., Milone et al. (2012, 2013, 2015a, b), Bellini et al. (2017). Moreover, the so-called “chromosome maps” (Milone et al. 2017) provide the means to clearly distinguish between different stellar populations, as well as sub-populations, in many GCs. For the most part, these separations are caused by chemical differences (mainly of C and N), though, with the right filter choices, stellar populations that have differ-

\* E-mail: vandenberg@uvic.ca

ent abundances of Mg can also be revealed (Milone et al. 2020). Importantly, precise photometry can yield tight constraints on He abundance variations within GCs (Milone et al. 2012, King et al. 2012, Nardiello et al. 2015), which are otherwise very difficult to determine.

Helium differs from the metals that are often described as the “light elements” (those below the iron-peak elements in the Periodic Table) in that it mainly affects the temperatures and luminosities of stars. At a given effective temperature ( $T_{\text{eff}}$ ), the bolometric corrections (BCs) that are relevant to old stellar populations have very little sensitivity to the He abundance (Girardi et al. 2007). On the other hand, stellar evolutionary computations (see, e.g., Salaris et al. 2006, Pietrinferni et al. 2009, Vandenberg et al. 2012, Cassisi et al. 2013) have shown that the locations of stars on the H-R diagram are essentially independent of the abundances of the light elements if, as seems to be the case in most GCs (e.g., Ivans et al. 1999, Cohen & Meléndez 2005), C+N+O and Mg+Al+Si are approximately constant. However, BCs can be very dependent on the actual abundance of each metal (depending on which spectral features are located within the passbands of the selected filters and the strengths of those features). For instance, variations in the abundances of C, N, and O, as manifested through the formation of CN, CH, NH, OH, and other molecules, can have significant effects on the fluxes in the Johnson-Cousins  $U$  and  $B$  filters (see Sbordone et al. 2011, their Fig. 4). Thus the complex morphologies and the large colour spreads that characterize many recent CMDs are almost entirely the consequence of BCs instead of variations in  $T_{\text{eff}}$ .

The Wide Field Camera 3 (WFC3) photometry that has been obtained via the *HST* UV Legacy Survey (Piotto et al. 2015, Nardiello et al. 2018, hereafter NLP18) provides a tremendous resource for the testing, and application, of stellar models. This survey was designed to use the  $F275W$ ,  $F336W$ ,  $F438W$ ,  $F606W$ , and  $F814W$  filters to obtain observations that would discriminate between stars with different abundances of He, C, N, and O. The availability of these data provided the main motivation for Vandenberg et al. (2021, hereafter Paper I) to compute stellar models for several different mixtures of the metals, including, in particular, different C:N:O ratios for two values of [CNO/Fe].

These computations employ BCs that are based on new MARCS high-resolution synthetic spectra which incorporate improved treatments of molecules that involve atoms of C, N, and O. The first application of these models, to the metal-rich GC NGC 6496, indicated that isochrones which employ the new BCs are able to reproduce observed colours at UV and optical wavelengths very well, possibly to within the uncertainties associated with the zero points of both the synthetic and observed photometry and the cluster properties (distance, reddening, metallicity). By comparison, isochrones employing the BCs derived from the previous generation of MARCS spectra (Gustafsson et al. 2008) fail to match the observed  $m_{F336W} - m_{F438W}$  colours by  $\gtrsim 0.12$  mag (though much smaller differences are obtained for redder colours). In addition, as shown by Martins et al. (2017), isochrones coupled with BCs based on Kurucz ATLAS12 model atmospheres (Kurucz 2014) and synthetic spectra as produced by the SYNTH code (Kurucz 2005) appear to predict too much flux at short wavelengths, resulting in, e.g.,  $M_{F336W}$  magnitudes that are too bright by  $\gtrsim 0.12$  mag and UV-optical colours that are too blue by similar amounts.

In this investigation, isochrones from Paper I are applied to the *HST* UV Legacy observations of six GCs that span the range in [Fe/H] from  $\sim -0.7$  to  $\sim -2.3$ . The two main goals of this project

are (i) an evaluation of the quality of our BCs and stellar models in both an absolute and a systematic sense, and (ii) an improved understanding of the chemical properties of the selected clusters. As we consider metal abundance mixtures that span close to the maximum range in CN abundances, at a given value of [CNO/Fe], as well as very wide variations in the abundances of C, N, and O, our focus is on comparisons of isochrones with the overall spreads in colours along the MS and lower RGB in observed CMDs. We consider this work to be a necessary first step towards the greater goal of evaluating the absolute light element abundances of the subpopulations of stars that have been revealed by chromosome maps. Accordingly, no attempt is made in this study to analyze such maps. (As an understanding of our results relies quite heavily on the material presented in Paper I, it is important that Paper I be read prior to this study.)

## 2 METAL ABUNDANCE MIXTURES AND BOLOMETRIC CORRECTIONS

This investigation is concerned with just a subset of the cases considered in Paper I; specifically, those listed in Table 1. The names that have been given to the different mixtures, which are listed in the first column, describe the abundance variations and BCs that they represent. All of them begin with “a4” to indicate that they assume  $[\alpha/\text{Fe}] = 0.4$  for the  $\alpha$  elements, while the subsequent letters identify the main abundance difference that distinguishes each mixture. Thus, “CN” indicates reduced C and increased N abundances consistent with CN-cycling, while “CNN” is similar to “CN” except that even higher N is assumed, implying a larger value of C+N+O. Likewise, “a4ON” and “ONN” are indicative of mixtures that would be produced by efficient ON-cycling; the latter differs from the former only in assuming a higher abundance of nitrogen. The others allow for enhanced C by 0.4 dex ( $x_{\text{C}_p4}$ ), enhancements in both C and O ( $x_{\text{CO}}$ ), or increased O abundances by 0.2 or 0.4 dex ( $x_{\text{O}_p2}$  or  $x_{\text{O}_p4}$ , respectively).

Whereas the previous generation of MARCS models (Gustafsson et al. 2008) assumed the solar abundances given by Grevesse et al. (2007), the model atmospheres and improved synthetic spectra that were computed for Paper I adopted the solar mixture of the metals reported by Asplund et al. (2009). When the abundances of the  $\alpha$  elements are increased by 0.4 dex, we obtain the a4s08 and a4s21 mixtures, which have “08” or “21” in their names to indicate, in turn, the 2008 or 2021 MARCS models. For both of these cases, and all others that are listed in Table 1, numerical values of the abundances of several elements are provided on the usual scale in which  $\log N(\text{H}) = 12.0$ . (The abundances are given explicitly only for those elements for which the effects of altered abundances on BCs have been investigated. Although there are differences in the assumed He abundances between the a4s08 and a4s21 mixtures, as indicated in the table, Paper I has demonstrated that they affect the BCs at the level of only a few thousandths of a magnitude.) For the other cases (i.e., a4CN ... a4xO\_p4), the changes in the abundances relative to the standard  $[\alpha/\text{Fe}] = 0.4$  mixture are specified in dex along with upward- or downward-pointing arrows to indicate, in turn, enhanced or reduced abundances. (The effects on BCs of differences in the assumed microturbulent velocity,  $v_T$ , as noted in Table 1, are discussed in Paper I.)

As reported by Pietrinferni et al. (2009) and Cassisi et al. (2013), isochrones on the theoretical plane are not affected by variations in C:N at constant C+N+O; consequently, one can simply apply the BCs that are calculated for mixtures with different C:N

**Table 1.** The Adopted Chemical Abundance Mixtures

Names of BC Tables <sup>a</sup>	He	C	N	O	[CNO/Fe]	Mg	Si	$v_T^b$
<b>a4s08</b>	10.93	8.39	7.78	9.06	+0.28	7.93	7.91	2.0
a4s21	11.00	8.43	7.83	9.09	+0.28	8.00	7.91	f(g)
a4CN	–	↓ 0.3	↑ 0.50	–	+0.28	–	–	f(g)
a4CNN	–	↓ 0.3	↑ 1.13	–	+0.44	–	–	f(g)
a4ON	–	↓ 0.8	↑ 1.30	↓ 0.8	+0.28	–	–	f(g)
a4ONN	–	↓ 0.8	↑ 1.48	↓ 0.8	+0.44	–	–	f(g)
a4xC_p4	–	↑ 0.4	–	–	+0.38	–	–	f(g)
a4xCO	–	↑ 0.7	–	↑ 0.2	+0.61	–	–	f(g)
a4xO_p2	–	–	–	↑ 0.2	+0.44	–	–	f(g)
a4xO_p4	–	–	–	↑ 0.4	+0.62	–	–	f(g)

<sup>a</sup> Boldface font identifies reference models (see the text); the others involve changes to the abundances of one or more of the metals, as tabulated, or to  $v_T$ .

<sup>b</sup> f(g) implies that the microturbulent velocity,  $v_T$ , varies with gravity such that  $v_T = 1.0$  km/s if  $\log g \geq 4.0$  or 2.0 km/s if  $\log g \leq 3.0$ .

ratios to the isochrones for the a4s21 abundances of C, N, and O (scaled to the [Fe/H] values of interest). Paper I confirmed and extended this result to stellar models of very low mass, though it also showed that the  $T_{\text{eff}}$ s of lower main-sequence (LMS) stars depend on the abundance of oxygen (and carbon, but to a lesser extent). It is therefore necessary, if one is interested in LMS stars, to take into account the effects of assumed C and O abundance variations on both the model temperatures and the BCs that are used to predict the magnitudes and colours of stars. In this investigation, Victoria-Regina (V-R) isochrones for  $[\alpha/\text{Fe}] = 0.4$  have been transformed to observed CMDs using the a4s21 BCs to represent CN-weak stars and the a4CN BCs to represent CN-strong stars. Similarly, we have applied the a4xO\_p2 or a4CNN BCs to stellar models for  $[\text{O}/\text{Fe}] = 0.6$ , with  $[m/\text{Fe}] = 0.4$  for the other  $\alpha$  elements, to represent CN-weak and CN-strong stars that have higher N (and hence higher C+N+O) abundances. Even though it was not necessary to compute grids of stellar models for the a4CN and a4CNN mixtures, they were generated for these and all of the other “a4” mixtures that are listed in Table 1 using the same code that is described by VandenBerg et al. (2012).

Paper I has already provided quite a detailed description of the procedure that is used to transpose isochrones from the theoretical plane to the various CMDs, but it is worthwhile to include a brief summary of what was done here. To keep the total computational effort at a manageable level, model atmospheres, synthetic spectra, and BCs were generated only for quite a sparse grid of parameter values; specifically,  $\log g = 1.0, 2.0, 3.0, 4.0, 4.5, 4.7, 5.0$ , and 5.3, with 4–6  $T_{\text{eff}}$  values at each gravity, for each of three metallicities ( $[\text{Fe}/\text{H}] = -2.5, -1.5$ , and  $-0.5$ ). The grid values of  $T_{\text{eff}}$  were determined from a consideration of isochrones for the selected [Fe/H] values. Tables were produced that contain not only these BCs (for each of the metal abundance mixtures), but also those based on 2008 MARCS spectra at the same parameter values; the latter were given the name a4s08 and derived from the transformation tables provided by Casagrande & VandenBerg (2014, hereafter CV14). These tables make it possible to evaluate the differences in the BCs between any of the “a4” tables, in turn, and the reference a4s08 dataset at common values of  $T_{\text{eff}}$ ,  $\log g$ , and [Fe/H]. Indeed, for a given isochrone, the BCs for the predicted temperatures at each of the grid values of  $\log g$  can be evaluated, and the resultant  $\delta(\text{BC})$  values as a function of  $\log g$  fitted by cubic splines for subsequent interpolations.

The transformation of isochrone luminosities and temperatures to magnitudes and colours involves the following steps. First, the BCs for the selected filters are derived from the CV14 tables, as they are provided for much finer spacings of  $T_{\text{eff}}$ ,  $\log g$ , and [Fe/H] than the BCs that have been computed for this project. Second, splines are fitted to the differences in the BCs for the selected mixture of the metals and the subset of the CV14 results that are contained in the a4s08 tables. Third, the splines are interpolated to yield the  $\delta(\text{BC})$  values at all intermediate values of  $T_{\text{eff}}$  and  $\log g$  along the isochrone (or extrapolated if  $\log g < 1.0$  or  $> 5.0$ ). Finally, the resultant  $\delta(\text{BC})$  values are applied to the isochrone that was generated in the first step of this process. Three-point (quadratic) interpolation is used to derive the transformations for any metallicity within the range  $-2.5 \leq [\text{Fe}/\text{H}] \leq -0.5$ . (Plots that illustrate the spline fits to the  $\delta(\text{BC})$  values and comparisons of isochrones that are generated in the first and fourth steps of this procedure are provided in Paper I.)

In what follows, the names listed in the first column of Table 1 are used to refer to the metal abundance mixtures, to the BCs, or to the isochrones for those mixtures.

### 3 APPLICATION OF STELLAR MODELS TO GLOBULAR CLUSTER CMDs

The photometric data for all of the GCs considered in this paper were released into the astronomical community by NLP18 via the website that they have provided. We have opted to use their “Method 1” photometry, which is preferred for the upper MS and more evolved stellar populations. Moreover, the CMDs were limited to stars with membership probabilities  $\geq 98\%$ , photometric errors  $< 0.02$  mag, and quality of fit (QFIT) parameters  $\geq 0.99$ , though these criteria were relaxed or tightened somewhat in order that the number of selected stars was sufficient to produce well-defined sequences from the upper MS to the lower red-giant branch (RGB). The MS and TO observations were sorted into 0.1 mag bins in  $m_{F606W}$ , and median fiducial points were determined for each bin. By fitting isochrones to the median fiducial sequence instead of the entire distribution of the individual stars in the vicinity of the TO, subjective errors associated with the determination of the best estimate of the TO age that corresponds to an adopted distance modulus are essentially eliminated.

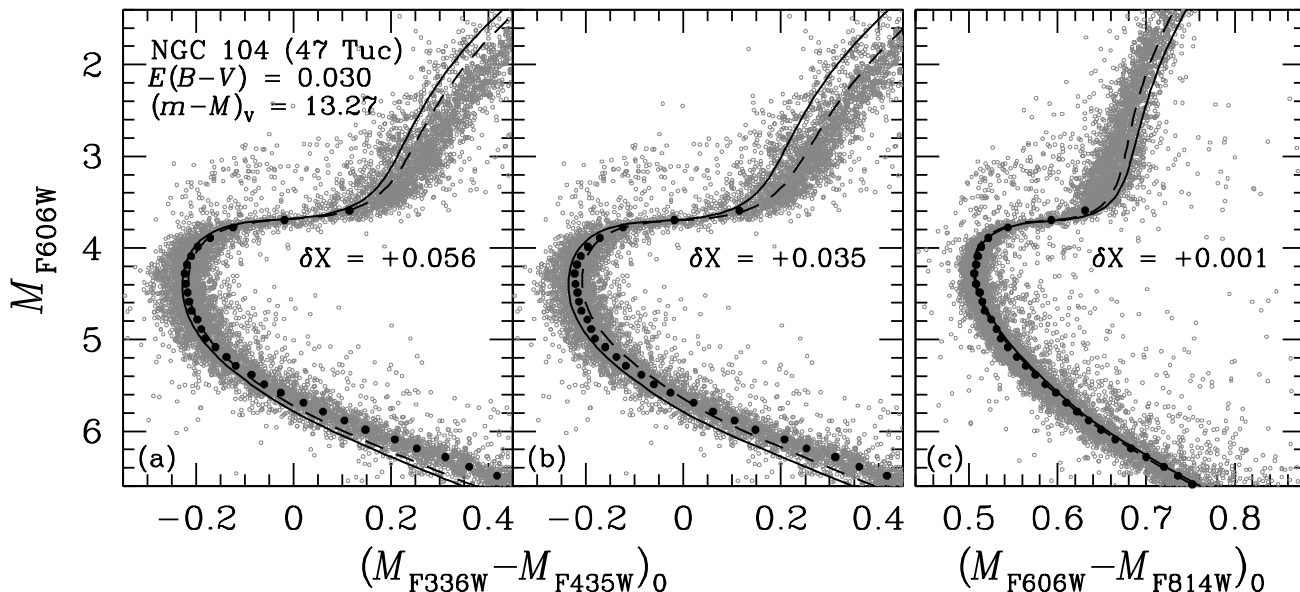


**Figure 1.** *Panel (a):* Fit of 12.5 Gyr isochrones for  $[\text{Fe}/\text{H}] = -0.70$ ,  $Y = 0.27$ , and  $[\alpha/\text{Fe}] = 0.4$  to observations of 47 Tuc (from NLP18), on the assumption of the indicated reddening and apparent distance modulus. (47 Tuc is the only GC considered in this study for which NLP18 provide ACS  $F435W$ , instead of WFC3  $F438W$ , magnitudes.) The isochrones have been transformed to the observed plane using the a4s21 and a4CN BCs, resulting in the solid and dashed curves, respectively. In order to fit the median fiducial sequence in the vicinity of the TO, the specified value of  $\delta X$  was applied to the isochrone colours (see the text). *Panel (b):* As in panel (a) except that the isochrones assume an age of 12.0 Gyr and a higher oxygen abundance by 0.2 dex; consequently, the solid and dashed curves employed the BCs for, in turn, the a4x0\_p2 and a4CNN mixtures (see Table 1). *Panel (c):* As in panel (b) except that the isochrones have been fitted to  $F606W, F814W$  photometry.

We have deliberately selected several GCs for this study that have been the subject of recent investigations in which the cluster distance moduli were obtained either from fits of zero-age horizontal branch (ZAHB) loci to the observed HB populations (e.g., Vandenberg et al. 2013, hereafter VBLC13, Vandenberg et al. 2016) or from full simulations of the latter (e.g., Denissenkov et al. 2017). In all such studies, the HB models provide fully consistent extensions of the Victoria-Regina isochrones (Vandenberg et al. 2014) to the core He-burning phase. To ensure that the results obtained in this study are compatible with those of previous investigations, we have adopted the same, or very similar, values of  $(m - M)_V$ ,  $E(B - V)$ , and  $[\text{Fe}/\text{H}]$ . These choices can be justified by the fact that the Victoria-Regina isochrones satisfy the constraints provided by, e.g., solar neighborhood Population II stars (Vandenberg et al. 2010), the morphologies of GC CMDs (see the aforementioned papers as well as, e.g., Correnti et al. 2016, Saracino et al. 2018), and the properties of cluster binaries (e.g., Brogaard et al. 2017, Vandenberg & Denissenkov 2018). Furthermore, the distance moduli that have been derived from the HB models agree rather well with those inferred from the RR Lyrae standard candle (e.g., VBLC13, Denissenkov et al. 2017).<sup>1</sup>

Our focus is on several of the CMDs that can be constructed from  $F336W$ ,  $F438W$ ,  $F606W$ , and  $F814W$  photometry. Because the MARCS spectra do not extend sufficiently far into the UV,

it was not possible to calculate BCs for the  $F275W$  filter; consequently, we are unable to fit isochrones to the available  $F275W$  observations. It should be noted as well that, although the CMD plots specify the values of  $E(B - V)$  and  $(m - M)_V$  that have been adopted for each GC, the excess in a given  $\zeta - \eta$  colour or the extinction  $A_\zeta$  has been calculated from the *nominal*  $E(B - V)$  value using the values of  $R_\zeta = A_\zeta/E(B - V)$  given by CV14 (their Table A1). Thus, for instance, the difference between the apparent and the absolute  $F606W$  magnitudes, which are plotted along the y-axis, can be easily calculated from  $(m - M)_{F606W} = (m - M)_V + (R_{F606W} - R_V)E(B - V)$ .

### 3.1 NGC 104 (47 Tuc)

With an absolute integrated visual magnitude of  $-9.42$  according to the 2010 edition of the Harris (1996) catalogue, 47 Tuc is one of the most massive GCs in the Milky Way. Its basic parameters appear to be quite well established. Brogaard et al. (2017) concluded from an examination of the available evidence that the best estimate of the foreground reddening is  $E(B - V) = 0.030 \pm 0.01$ , and their analysis of an eclipsing binary member known as V69 suggested a preference for  $[\text{Fe}/\text{H}] = -0.70$ ,  $[\alpha/\text{Fe}] = 0.4$ ,  $[\text{O}/\text{Fe}] \approx 0.6$  and  $Y \approx 0.25$ . (By comparison, the latest spectroscopic survey gives  $[\text{Fe}/\text{H}] = -0.76$ ; see Carretta et al. 2009a, hereafter CBG09.) V69 could well be a member of a helium-poor population given that simulations of the cluster HB stars by Denissenkov et al. (2017) have indicated that the star-to-star variation of the initial He abundance in 47 Tuc is  $\delta Y_0 \approx 0.03$ , with a mean value close to 0.27. The same simulations yield  $(m - M)_V = 13.27$  if the metallicity is taken to be  $[\text{Fe}/\text{H}] = -0.70$  and the faintest HB stars have  $Y_0 = 0.257$ . This is in very good agreement with the determination of  $(m - M)_V = 13.30$  by Brogaard et al. from the binary V69, and with the true modulus

<sup>1</sup> As a further check of the ZAHB-based distance scale, we compared the true distance moduli that were derived by VBLC13 from fits of ZAHB models to the HB populations of 43 GCs with the results reported by Baumgardt & Vasiliev (2021), which are based on Gaia EDR3 parallaxes and their compilation of literature values. For 27 (63%) of the clusters, the differences in  $(m - M)_0$  are  $\leq 0.05$  mag; only for 6 of the GCs are the differences  $> 0.10$  mag.

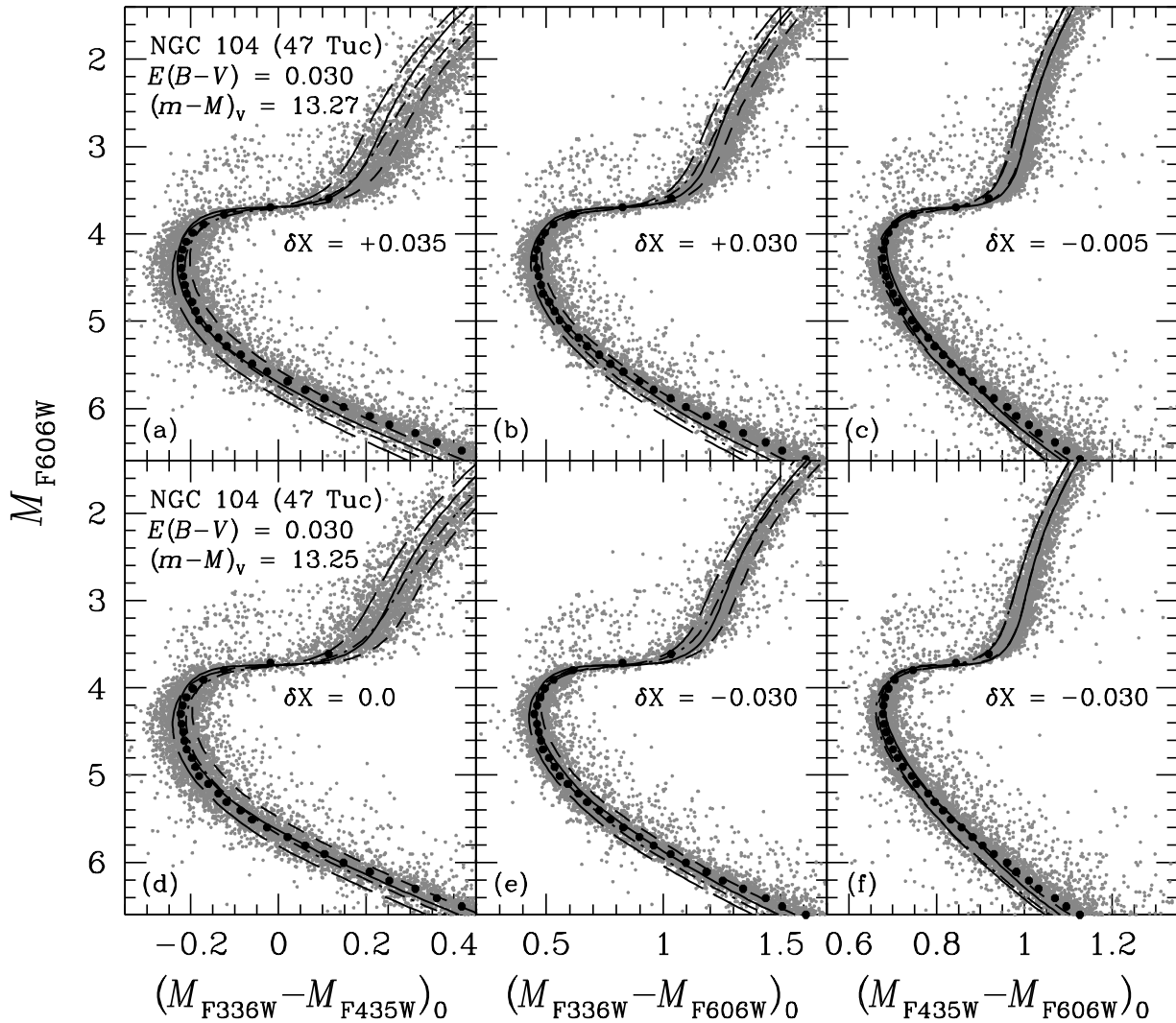


**Figure 2.** Panels (a)–(c): As in the middle and right-hand panels of the previous figure, except that the isochrones represented the solid and dashed curves assume  $Y = 0.25$ , while those plotted as the long-dashed and dot-dashed loci assume  $Y = 0.30$ . Panels (d)–(f): As in panels (a)–(c), except that the isochrones assume  $[\text{Fe}/\text{H}] = -0.60$  and an age of 11.9 Gyr.

derived by Chen et al. (2018),  $(m - M)_0 = 13.24 \pm 0.06$ , if  $A_V \lesssim 0.09$  mag. (As the distance reported by Chen et al. was obtained from Gaia DR2 parallaxes with a correction to the zero-point of the parallax scale based on observations of quasars and background stars in the Small Magellanic Cloud, it is independent of stellar models.)

In contrast with all other GCs considered in this study, NLP18 provide *HST* Advanced Camera for Surveys (ACS)  $F_{435W}$  photometry for 47 Tuc instead of WFC3  $F_{438W}$  data. However, this is of little consequence, as our isochrones indicate that predicted colours involving these magnitudes (e.g.,  $M_{F336W} - M_{F435W}$  versus  $M_{F336W} - M_{F438W}$ ) are nearly identical once a small zero-point difference ( $\approx 0.01$  mag) between the  $F_{438W}$  and  $F_{435W}$  BCs is taken into account. Of the various CMDs considered here, one can anticipate that the  $(M_{F336W} - M_{F435W})_0$ ,  $M_{F606W}$  diagram will provide the most challenging test of stellar models because the selected colour involves the UV filter,  $F_{336W}$ . According to Figure 1a, isochrones for  $[a/\text{Fe}] = 0.4$  that are relevant for CN-weak and CN-strong stars (the solid and dashed curves, respectively), have to be adjusted by quite a large amount in the horizontal direction (0.056

mag) in order to match the observed TO colour.<sup>2</sup> Furthermore, even when this offset is applied to the models, the isochrones fail to reproduce the CMD locations of the lower RGB stars. (Note that the adopted correction to the colours was chosen so that the isochrones would straddle the median fiducial sequence in the vicinity of the TO; this was done on purpose to reflect the fact that the distribution of CN strengths is known to be strongly bimodal in 47 Tuc; see, e.g., Cannon et al. 1998, their Fig. 3.)

However, as shown in Fig. 1b, isochrones for a higher abundance of oxygen by 0.2 dex, as transformed to the observed plane

<sup>2</sup> NLP18 tabulate the uncertainties in the photometric zero-points that are used to calibrate instrumental magnitudes in the VegaMag system. For most clusters, they are at the level of 0.01–0.02 mag for  $F_{275W}$  and the other WFC3 filters, implying possible colour errors of  $\sim 0.014$ – $0.028$  mag. This could well be responsible for part of the  $\delta X$  offsets that are needed to reconcile predicted and observed TO colours, but they may also be the result of errors in the model  $T_{\text{eff}}$  scale and in the  $\text{BC}-T_{\text{eff}}-[\text{Fe}/\text{H}]$  relations, both of which are hard to quantify, as well as to errors in the assumed cluster properties (i.e., metallicities, distances, and foreground reddenings).

using the a4x0\_p2 BCs to represent CN-weak stars (solid curve) and the a4CNN BCs to represent CN-strong stars (dashed curve) provide significantly improved fits to the observed CMD. The colour offset,  $\delta X$ , has been reduced to 0.035 mag and the overlay of the model loci onto the cluster giants has improved, though the stellar models are still too blue. (Presumably both of these discrepancies between theory and observations would be even smaller if isochrones for  $[O/Fe] > 0.6$  were fitted to the observations, but there is no (other) evidence for such high oxygen abundances at  $[Fe/H] \gtrsim -0.7$ .) One of the consequences of a 0.2 dex increase in the O abundance is a modest reduction in the TO age to  $\approx 12.0$  Gyr from  $\approx 12.5$  Gyr (in panel a), if the same apparent distance modulus is adopted.

Fig. 1c has been included here to show that the same isochrone loci that appear in panel (b) provide superb fits to the  $(M_{F606W} - M_{F814W})_0$  colours of the upper MS and TO stars in 47 Tuc without requiring a significant adjustment to the predicted colours. This argues against the possibility that the differences between the predicted and observed colours in Fig. 1b are mainly due to problems with the model  $T_{\text{eff}}$  scale. As regards the discrepancies along the lower RGB: the relative locations of the solid and dashed curves indicate that  $F606W, F814W$  photometry is sensitive to the abundance of nitrogen. Since our models for the a4CNN mixture assume  $[N/Fe] = 1.13$ , as compared with measured abundances that range up to  $[N/Fe] \sim +1.6$  (see Briley et al. 2004, their Fig. 6; Cohen et al. 2005, their Fig. 11), computations for higher N abundances may do a better job of reproducing the colours of the bluest giants. Further work is needed to investigate this possibility.

The difficulties that are apparent in Fig. 1 can be alleviated to a considerable extent by allowing for He abundance variations. Helium mainly affects the predicted gravities and temperatures of stars. It has almost no impact on the BCs at fixed values of  $[Fe/H]$ ,  $T_{\text{eff}}$ , and  $\log g$  — something that was verified in Paper I by comparing BCs for the same mixtures of the metals, but different  $Y$  (also see Girardi et al. 2007). In fact, a star-to-star He abundance variation corresponding to  $\delta Y \sim 0.05$ , which is on the high side for most GCs, is predicted to have almost no effect on the  $M_{F336W} - M_{F435W}$  colours of TO stars, while causing a spread of the same colour along the MS and lower RGB by  $\sim 0.04$ – $0.06$  mag. This is shown in Figure 2a, which plots 12.0 Gyr isochrones for the same oxygen-enhanced abundances as in Fig. 1b, but for  $Y = 0.25$  and  $0.30$ . Along the giant branch, the horizontal separation between the solid and long-dashed isochrones, or between the dashed and dot-dashed loci, is about half of that predicted by the models that represent CN-weak and CN-strong stars (e.g., the solid and dashed isochrones) at constant  $Y$ . Figs. 2b and 2c show that the same isochrones provide comparable fits to other CMDs that can be constructed from  $F336W, F435W$ , and  $F606W$  photometry.

Clearly, variations in both  $Y$  and CN should be taken into account when attempting to explain the observed widths, at a given magnitude, of both the MS and the lower RGB of 47 Tuc. In fact, our models are able to explain the *thicknesses* of the principal photometric sequences quite well if  $\delta Y \sim 0.05$ . The main difficulty with the stellar models is that they are generally too blue along the lower RGB (in all three of the CMDs that have been plotted). One possible way of improving the fits to the observations is to adopt a higher metallicity (i.e.,  $[Fe/H] > -0.70$ ), which has been found in some spectroscopic studies (see, e.g., Carretta et al. 2004, Wylie et al. 2006, Johnson et al. 2015). As shown in Figs. 2d–f, isochrones for a higher  $[Fe/H]$  value by 0.1 dex provide better fits to the cluster giants by virtue of being cooler and therefore redder; indeed, the region enclosed by the bluest and reddest isochrones contains

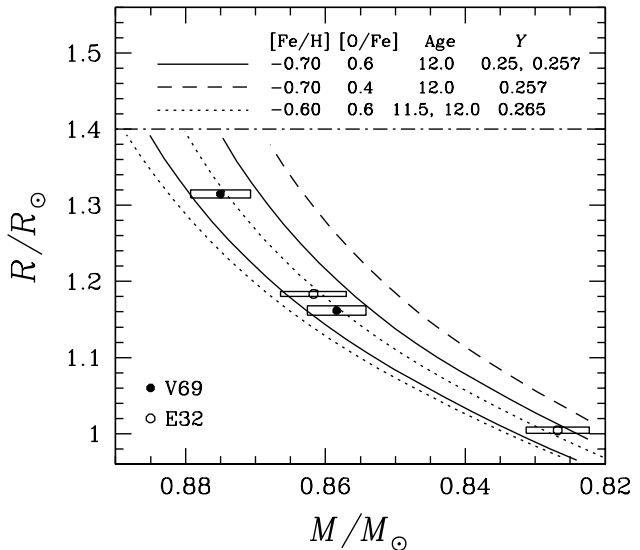


**Figure 3.** Comparison of the predicted relations between mass and radius from several isochrones that have the indicated ages and chemical abundances with the properties of the eclipsing binaries V69 and E32 in 47 Tuc (filled and open circles, respectively, and the associated error boxes). Their masses and radii were taken from the study by Thompson et al. (2020). The adopted value of  $[O/Fe]$  is given explicitly; all other  $\alpha$ -elements are assumed to have  $[m/Fe] = 0.4$ .

most of the MS, TO, and giant-branch stars. These models also require less of a redward shift of their  $M_{F336W} - M_{F435W}$  colours to match the observed TO, though similar or larger colour adjustments are needed in the case of the other colours. It would therefore appear that isochrones for an intermediate metallicity (say,  $[Fe/H] \approx -0.65$ ), together with a higher nitrogen abundance than in our current models, would provide the best overall fits to the various CMDs. (Note that ZAHB models for  $[Fe/H] = -0.60$  yield a smaller value of  $(m - M)_V$  by 0.02 mag and that the best estimate of the corresponding TO age is just slightly reduced to 11.9 Gyr.)

Fortunately, member eclipsing binary stars provide important constraints on the chemical composition of 47 Tuc. Thompson et al. (2020) have recently reduced (albeit only slightly) the uncertainties associated with the physical properties of V69, as compared with the findings of Brogaard et al. (2017), and they have determined precise masses and radii for a second binary, E32, to within 0.55% and 0.40%, respectively. Their results for the two binaries are compared with the  $M$ – $R$  relations from several isochrones in Figure 3. The solid curve located to the left of the binary components, which predicts higher masses at a given radius, represents the same isochrone (for  $Y = 0.25$ ) that was fitted to the 47 Tuc photometry in Figs. 2a–c, while the other one assumes  $Y = 0.257$ . These results show that a relatively low He abundance ( $0.250 \lesssim Y \lesssim 0.257$ ) is required by the binary constraint if 47 Tuc has  $[Fe/H] = -0.70$ ,  $[O/Fe] = 0.6$  (with  $[m/Fe] = 0.4$  for the other  $\alpha$  elements), and an age near 12.0 Gyr. The assumption of a higher O abundance (and hence higher  $[CNO/Fe]$ ) would shift the predicted  $M$ – $R$  relations further to the left, in which case, the binaries would favor a somewhat higher  $Y$ . (This would actually be more consistent with expectations for a relatively metal-rich GC if  $\delta Y/\delta Z \gtrsim 1$  as the result of chemical evolution since the Big Bang.)

By comparison, the dotted curves represent isochrones for the same  $[Fe/H]$  value ( $-0.60$ ) and the oxygen-enhanced mixture of the metals that were plotted in Figs. 2d–f, though we have assumed  $Y =$

0.265 for the He abundance so that a 12.0 Gyr isochrone provides a good fit to the properties of the binary components. The dotted curve that lies furthest to the left in this plot shows the effect on the  $M$ – $R$  relation of a reduction in the age by 0.5 Gyr. The horizontal shift between the two dotted loci is apparently nearly the same as that caused by  $\delta Y \approx 0.007$ , which is responsible for the separation at constant radius between the two solid curves.

The dashed curve in Fig. 3 is of particular importance because it has been derived from a 12.0 Gyr isochrone for  $[\text{Fe}/\text{H}] = -0.70$ ,  $Y = 0.257$ , and  $[\text{O}/\text{Fe}] = [\alpha/\text{Fe}] = 0.4$ . It is clearly problematic insofar as it predicts masses for the binary at the observed radii that are too low. (In fact, this isochrone would match the observed TO luminosity only if a larger distance modulus by  $\sim 0.07$  mag were adopted. Smaller values of  $(m - M)_V$  would imply higher ages and reduced masses.) This is the reason why Brogaard et al. (2017) favoured a higher O abundance if the metallicity of 47 Tuc is  $[\text{Fe}/\text{H}] = -0.70$ . Although the distance modulus uncertainty permits some flexibility in the fits to the mass-radius diagram, we have been able to obtain a consistent interpretation of both the WFC3 CMDs of 47 Tuc and its eclipsing binaries on the assumption of  $[\text{Fe}/\text{H}] \gtrsim -0.70$  and  $[\text{O}/\text{Fe}] \sim 0.6$ . The small discrepancies that remain between predicted and observed colours, in particular, may well be reduced if we were to adopt alternative choices for the abundances of the CNO elements and/or though further improvements to the computation of synthetic spectra and BCs — but this must be left for future work to determine. Perhaps the main point of our analysis is that star-to-star variations in the abundances of just the three elements, He, C, and N appear to be able to account for most of the observed colour spreads along the MS and RGB of 47 Tuc.

In concluding this section, some discussion is warranted concerning the fact that the isochrones which were fitted to the CMDs of NGC 6496 in Paper I required much smaller colour offsets ( $\lesssim 0.01$  mag) than those obtained for 47 Tuc, despite having a similar metallicity to within  $\sim 0.2$  dex. We suspect that the most likely explanation of this difference is that the photometry of NGC 6496 was fitted by models that assumed  $[\alpha/\text{Fe}] = 0.4$ , which is probably too high. As this cluster has  $[\text{Fe}/\text{H}] \gtrsim -0.5$  (CBG09), it would be expected to have  $[\alpha/\text{Fe}] \sim 0.25$  if it lies close to the standard relation between  $[\alpha/\text{Fe}]$  and  $[\text{Fe}/\text{H}]$  that has been derived for field Population II stars (e.g., Edvardsson et al. 1993, Fuhrmann 2008). Indeed, we have verified, using V-R isochrones and the BCs provided by CV14, that the models for lower abundances of the  $\alpha$  elements by  $\sim 0.15$  dex would require redward colour shifts that are similar to those found for 47 Tuc. However, differences in the C+N+O abundance between NGC 6496 and 47 Tuc could also affect how well stellar models are able to reproduce their respective TO colours.

### 3.2 NGC 6362

NGC 6362 should be a particularly good GC for the testing and calibration of stellar models for  $[\text{Fe}/\text{H}] \sim -1.0$  because it contains a large number of RR Lyrae variables, as well as eclipsing binaries with well determined properties. In their recent study of this system, VandenBerg & Denissenkov (2018) found that these constraints could be satisfied quite well if NGC 6362 has  $E(B - V) = 0.07$ – $0.08$ , which is consistent with the reddenings derived from dust maps (Schlegel et al. 1998, Schlafly & Finkbeiner 2011), and an apparent distance modulus in the range of  $(m - M)_V = 14.56$ – $14.60$ , if the cluster has  $-1.0 \lesssim [\text{Fe}/\text{H}] \lesssim -0.85$ . Although many spectroscopic studies have found metallicities somewhat below  $-1.0$ , including the surveys by Kraft & Ivans (2003) and CBG09, the binary stars appear to preclude such low values if they have

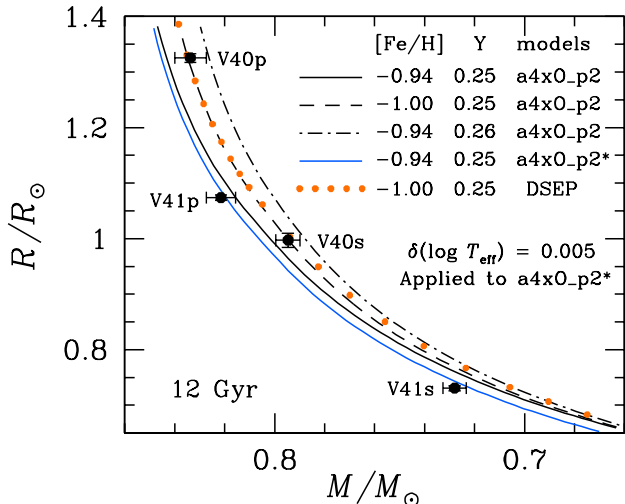


**Figure 4.** Comparison of the  $M$ – $R$  relations predicted by 12 Gyr isochrones that have the indicated chemical abundances with the properties of the eclipsing binaries (V40 and V41) in NGC 6362 (filled circles and error bars) as derived by Kaluzny et al. (2015). The only difference between the solid curves in blue and black is that the predicted temperatures along the former were arbitrarily increased by  $\delta \log T_{\text{eff}} = 0.005$ , resulting in smaller radius at fixed luminosities. An isochrone from the Dartmouth (DSEP) database (Dotter et al. 2008) for very close to the same metal abundances as the a4x0\_p2 models (see the text) has also been plotted (small filled circles in orange).

$Y_0 \gtrsim 0.25$  and  $[\text{O}/\text{Fe}] \lesssim 0.6$ . Simulations of the cluster HB that were presented in the same paper by VandenBerg and Denissenkov indicated that the initial He abundance varies by  $\delta Y_0 \approx 0.03$ , with  $\langle Y_0 \rangle \approx 0.26$ .

To illustrate the difficulties presented by the eclipsing binaries for  $[\text{Fe}/\text{H}] \lesssim -1.0$ , we have plotted in Figure 4 the masses and radii of the binaries V40 and V41, together with the uncertainties in these properties, from the study by Kaluzny et al. (2015). Superimposed on the observations are the predicted mass-radius relations from 12 Gyr isochrones for the a4x0\_p2 mixture, assuming the indicated values of  $Y$  and  $[\text{Fe}/\text{H}]$ . (An age close to 12 Gyr is expected if NGC 6362 has an apparent distance modulus close to  $(m - M)_V = 13.60$ ; see below.) The solid curve in black shows that the properties of the primary of V41 can be matched by isochrones for  $Y = 0.25$ , which should be very close to the minimum possible value because it is approximately the primordial He abundance (Cyburt et al. 2016), only if  $[\text{Fe}/\text{H}] \gtrsim -0.94$  is assumed. (It is much easier to accommodate either a somewhat lower metallicity or a higher He abundance in the case of V40; note its location relative to the dashed and dot-dashed curves.) If the adopted metallicity is decreased by as little as 0.06 dex, the corresponding  $M$ – $R$  relation (the dashed curve) is well outside the  $1\sigma$  error box of V41p. Although not shown, nearly the same relation as the dashed curve is obtained if the O abundance is decreased by 0.2 dex (to  $[\text{O}/\text{Fe}] = 0.4$ ). These results provide ample justification for adopting  $[\text{O}/\text{Fe}] = 0.6$  in the fits of isochrones to the cluster CMDs to be presented shortly.

The small filled circles in orange, which represent the  $M$ – $R$  relation predicted by an isochrone from the Dartmouth database (Dotter et al. 2008) for the same age, metallicity, and He abundance as the dashed curve, but for  $[\alpha/\text{Fe}] = 0.4$ , demonstrate that our models agree quite well with the results of a completely independent stellar evolution code. Although the Dartmouth isochrones adopted the solar abundances reported by Grevesse & Sauval (1998) as

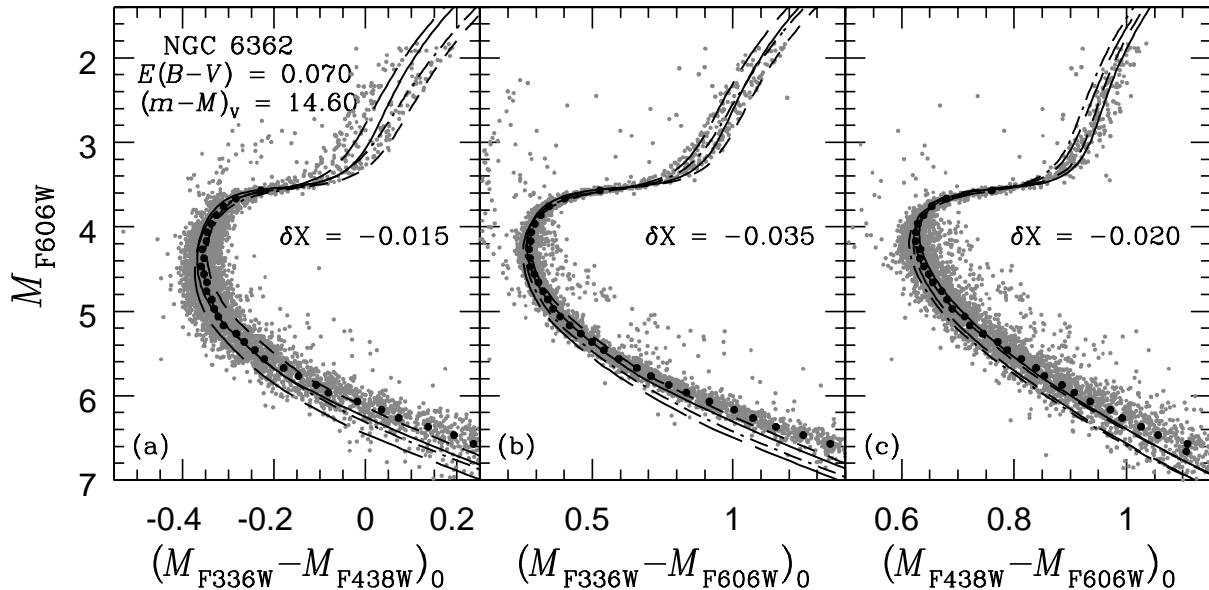


**Figure 5.** Similar to the top (or bottom) row of panels in Fig. 2; in this case, WFC3 observations of NGC 6362 (from NLP18) have been fitted by 11.8 Gyr isochrones for  $[\text{Fe}/\text{H}] = -0.94$ ,  $Y = 0.25$ ,  $[\alpha/\text{Fe}] = 0.4$ , and  $[\text{O}/\text{Fe}] = 0.6$  employing either the a4x0\_p2 or a4CNN BCs (solid and dashed curves, respectively). Otherwise identical isochrones, but for  $Y = 0.30$  are represented, in turn, by the long-dashed and dot-dashed loci.

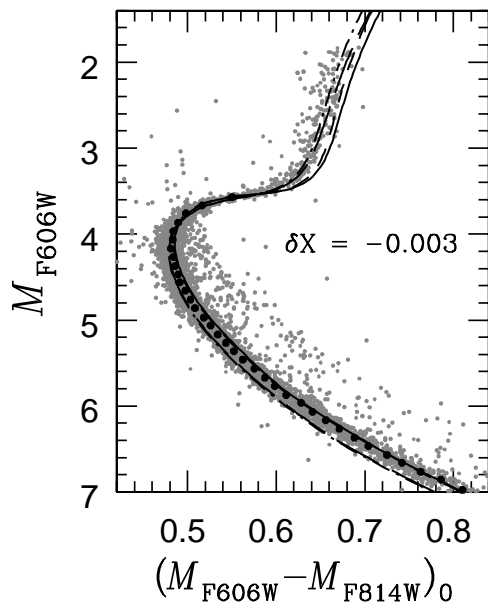


**Figure 6.** As in the previous figure, except that the isochrones have been fitted to WFC3  $F606W$ ,  $F814$  observations of NGC 6362.

the reference mixture of the metals, it turns out that their models for  $[\alpha/\text{Fe}] = 0.4$  assume nearly the same C+N+O abundance as our isochrones for  $[\text{O}/\text{Fe}] = 0.6$  and  $[m/\text{Fe}] = 0.4$  for the other  $\alpha$  elements; in fact, the two mixtures have the same value of  $\log(\text{C}+\text{N}+\text{O})$  to within 0.01 dex. This explains why the dashed and orange loci are so similar. Since both of these curves predict masses, at the derived radii of V41, that are significantly lower than the observed masses of this binary, it would appear to be quite a robust result that NGC 6362 has  $[\text{Fe}/\text{H}] \gtrsim -1.0$  and a high value of  $[\text{CNO}/\text{Fe}]$ .

Interestingly, V41 appears to lie along a different mass-radius

relation than V40, implying that the helium abundances of the two binaries differ by  $\delta Y \sim 0.01$ . However, it is clearly much more difficult to obtain a consistent interpretation of V41 than of V40, whose components can be fitted equally well by the same  $M$ - $R$  relation. Our isochrones apparently predict radii at the observed mass of V41s that are too large. This could be telling us that the temperatures of our stellar models are too high. If the a4x0\_p2 isochrone for  $[\text{Fe}/\text{H}] = -0.94$ ,  $Y = 0.25$ , and  $[\text{O}/\text{Fe}] = 0.6$  (the solid curve in Fig. 4) is arbitrarily shifted to higher  $T_{\text{eff}}$ s by  $\delta \log T_{\text{eff}} = 0.005$  (approximately 70 K at  $T_{\text{eff}} = 6000$  K), it provides a satisfactory fit to the properties of both components of V41. This is illustrated by the solid curve in blue. (A shift of the model loci in Fig. 4 to smaller radii would tend to increase the cluster He abundance as inferred from its binaries.) The possibility of temperature scale errors should be kept in mind as they are bound to be present at some level.

Fits of 11.8 Gyr isochrones for  $[\text{Fe}/\text{H}] = -0.94$ ,  $Y = 0.25$ ,  $[\alpha/\text{Fe}] = 0.4$ , and  $[\text{O}/\text{Fe}] = 0.6$  to the WFC3 CMDs of NGC 6362 are shown in Figures 5 and 6; the a4x0\_p2 and a4CNN BCs were used to generate the solid and dashed loci, respectively. The isochrone represented by long dashes assumes  $Y = 0.30$  but is otherwise identical to the solid curve. The clear separation of the lower RGB stars into two sequences is especially striking in the left-hand panel of Fig. 5. This could be the manifestation of a strong bimodality in CN strengths, at least in part. Indeed, this is suggested by the isochrones that have been superimposed on the observations.

However, although models that allow for variations in  $Y$  and CN strengths are able to match the full width of the RGB, at a given  $F606W$  magnitude, in panel (b), they are less successful in this regard in the other two panels. Moreover, they fail to explain the bluest giants in panel (a), or the reddest ones in panel (c), which cannot be attributed to errors in the model  $T_{\text{eff}}$  scale or to the assumed He abundances because they cannot cause a redward offset of the models in some CMDs and blueward shifts in others. (We defer our discussion of possible causes of this difficulty to our analyses of the M 5 and M 3 CMDs where the same

discrepancies between theory and observations are even more pronounced.) On the other hand, aside from the apparent differences between the predicted and observed MS slopes, our isochrones are able to reproduce the observed MS widths satisfactorily. As in the case of 47 Tuc, our isochrones provide good fits to the observed  $M_{F606W} - M_{F814W}$  colours of MS stars in NGC 6362, though they are too red along the giant branch (see Fig. 6).<sup>3</sup>

Encouragingly, the  $\delta X$  colour offsets that must be applied to the isochrones in order to match the observed TO colours are relatively small. The fact that they are all negative (i.e., the isochrones must be adjusted to bluer colours) does raise the concern that the adopted [Fe/H] value may be too high, as the differences between the predicted and observed colours would be less if lower metallicity, and therefore bluer, isochrones were fitted to the observations. Indeed, for most of the GCs considered in this study, the predicted  $M_{F336W} - M_{F438W}$  and  $M_{F336W} - M_{F606W}$  colours must be *increased* by small amounts in order to reproduce the observed colours — though the isochrones that are fitted to their CMDs assume [Fe/H] values that have stronger support from spectroscopy. In fact, we would have found the same thing for NGC 6362 (i.e., small positive colour offsets) had we adopted, say, [Fe/H] =  $-1.07$  (CBG09). However, if the cluster actually has a lower metallicity by  $\sim 0.1$  dex than we have assumed, consistent fits to both the photometric data and the eclipsing binaries would presumably require a higher C+N+O abundance than in our current stellar models (as already mentioned).

### 3.3 NGC 5904 (M 5)

With about half of the metallicity of NGC 6362, M 5 is a suitable cluster to consider as we extend our analyses to more metal-deficient systems in steps of  $\approx 0.3$  dex in [Fe/H]. Its basic parameters appear to involve rather little controversy. According to the spectroscopic survey by CBG09, M 5 has [Fe/H] =  $-1.33$ , and if ZAHB models for this metallicity and  $Y = 0.25$  are fitted to the cluster HB, one obtains  $(m - M)_V = 14.38$  (see, e.g., VBLC13). The reddening appears to be close to  $E(B - V) = 0.035$  insofar as this estimate is within 0.003 mag of the foreground reddening that are found from the Schlegel et al. (1998) and Schlafly & Finkbeiner (2011) dust maps. If 11.4 Gyr isochrones for the same O- and  $\alpha$ -enhanced mixture of the metals that was adopted for 47 Tuc and NGC 6362 are fitted to the WFC3 CMDs of M 5, we obtain the results shown in Figure 7.

The models for  $Y = 0.25$ , when converted from the theoretical to the observed planes using the a4x0\_p2 and a4CNN BCs, enclose the densest concentration of stars along the lower RGB in the left-hand panel particularly well. However, as in the case if NGC 6362, our models are unable to explain the bluest RGB stars (or the reddest stars in the right-hand panel). That is, the observed colour variations at a given  $M_{F606W}$  magnitude along the RGB are considerably larger than predicted by our isochrones. If the bluest giants have high He abundances,  $Y$  would have to be much greater than 0.30 (which was assumed in the isochrone that is represented

by long dashes). This seems highly improbable. Not only is a wide range in  $Y$  ruled out by the relatively narrow MS widths that are apparent in Figs. 7a and 7b, but the HB of M 5 is morphologically very similar to the HB of M 3, which can be modeled very well without requiring a large He abundance variation within the cluster (Denissenkov et al. 2017).

It is worth pointing out that, at the metallicity of M 5 (and lower [Fe/H] values; see Fig. 10 in Paper I), the  $M_{F336W} - M_{F438W}$  colours are predicted to have very little dependence on  $Y$  or the C:N:O abundances in the vicinity of the TO. Hence, there is presumably another explanation for the observed spread in this colour at  $M_{F606W} \sim 3.5\text{--}5$  (see Fig. 7a). Indeed, the same comment can be made to a greater or lesser extent with regard to the colours that are plotted in the other panels. Unless the actual abundance variations are much larger than we have assumed, we suspect that photometric errors are primarily responsible for the observed dispersion in the TO colours, with perhaps some contributions due to the presence of binaries and the effects of differential reddening (which is unlikely to be important in clusters with low  $E(B - V)$  values, like M 5). As we have concluded in our analyses of the M 92 CMDs in § 3.6, photometric scatter would seem to be the only viable explanation for similar colour spreads at the TOs of the lowest metallicity GCs.

Since chemical differences have much stronger effects on the BCs relevant to cool giants than to TO stars (see Paper I), the lower RGB stars of M 5 should be especially revealing. This cluster, as in the case of NGC 6362, seems to have a bifurcated giant branch on the  $(M_{F336W} - M_{F438W})_0, M_{F606W}$  diagram; see Figure 8a (the top, left-hand panel), which provides a magnified view of the SGB and lower RGB of M 5. The stars plotted as gray points can be explained by isochrones that allow for variations in CN strengths (with perhaps a modest variation in  $Y$ )— but not the bluer giants (the black points), which define a separate sequence of stars. The fact that the latter also tend to have redder  $(M_{F438W} - M_{F606W})_0$  colours than both the “normal” giants (see Fig. 8c) and, in particular, the isochrones in Fig. 7c, rules out the possibility that they have very high He abundances because, as shown in Fig. 7, stars with higher  $Y$  are predicted to have bluer RGBs on all three CMDs. Of the several metal abundance mixtures considered in this investigation, only those that have enhanced C abundances (see Fig. 7 in Paper I) seem to be able to account for the different behavior of the anomalous giants on the various CMDs.

The effects of high C are illustrated in bottom row of plots in Fig. 8, which superimpose the lower RGB portions of several isochrones onto the same CMDs that appear in the upper row. All of the models assume  $Y = 0.30$ , which is probably somewhat higher than the upper limit of the star-to-star He abundance variation in M 5. The dashed, solid, and long-dashed curves represent, in turn, isochrones for the basic a4x0\_p2 mixture, the a4xC\_p4 mix (i.e., increased C by 0.4 dex), and the a4xC0 mixture, in which C has been enhanced by 0.7 dex and O by 0.2 dex. Note, in particular, how well these three loci encompass the observed giants in Fig. 8g. The dashed curve matches the blue edge of the stars that have been plotted as gray points, suggesting that they are CN-weak stars with  $Y \approx 0.30$ , while the reddest giants are well matched by the models for [C/Fe] = +0.7, [O/Fe] = 0.6, and [m/Fe] = 0.4 for the other  $\alpha$  elements. (The only difference between the a4xC0 and a4x0\_p2 mixtures is the carbon enhancement of the former.) The a4xC\_p4 models, with [C/Fe] = +0.4, lie between those for the a4xC0 and a4x0\_p2 mixtures. (The inferred *variations* in the C abundances should be more trustworthy than the absolute abundances implied by the overlays of isochrones onto observed CMDs given the likelihood that the models are subject to a number of uncertainties

<sup>3</sup> Because the fits of isochrones to  $F606W, F814W$  observations of all of the GCs considered in this paper look so similar — i.e., the isochrones reproduce the CMD locations of MS and TO stars very well, with little or no offsets to the predicted colours, and they are always too red along the giant branch by  $\sim 0.03\text{--}0.04$  mag at a given absolute magnitude — we decided to include such plots in this paper only for 47 Tuc and NGC 6362. Similar plots for the other clusters considered in this investigation are qualitatively nearly identical and therefore do not add anything to our understanding.

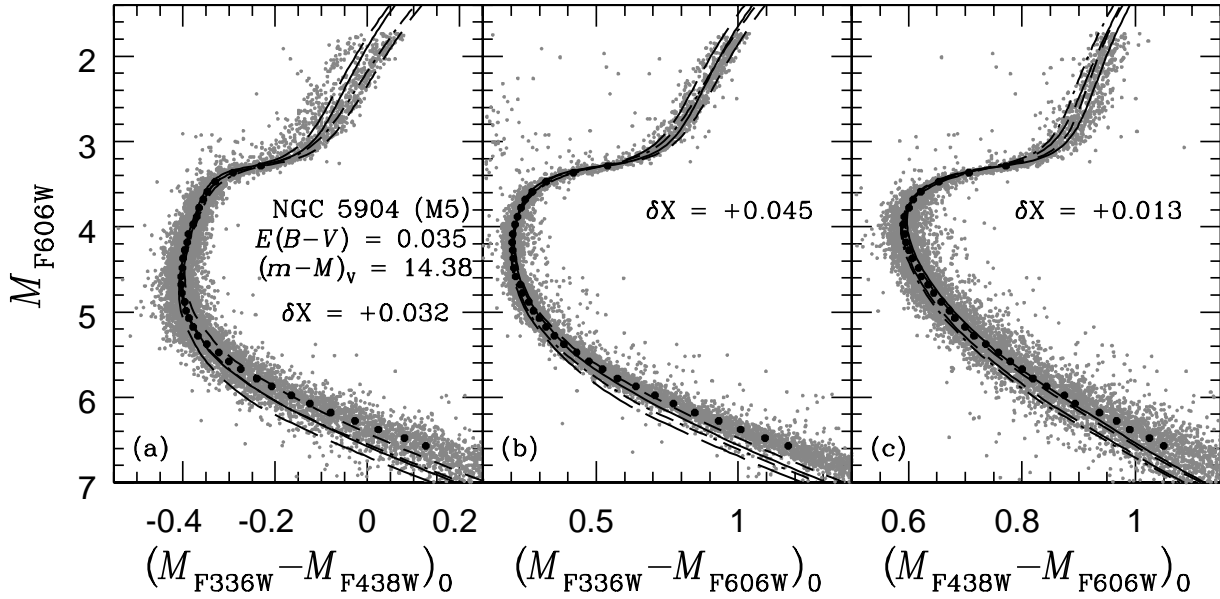


**Figure 7.** Similar to the previous figure; in this case, 11.4 Gyr isochrones for  $[\text{Fe}/\text{H}] = -1.33$ ,  $Y = 0.25$ ,  $[\alpha/\text{Fe}] = 0.4$ , and  $[\text{O}/\text{Fe}] = 0.6$  have been fitted to WFC3 observations of M5 (from NLP18) on the assumption of the indicated reddening and apparent distance modulus. The long-dashed and dot-dashed loci represent isochrones for  $Y = 0.30$  but are otherwise identical to the solid and dashed curves, respectively. Fits to  $F606W$ ,  $F814W$  photometry (not shown) look very similar to those given in Fig. 1c; in this case, the models match the MS and TO observations without requiring any adjustments to the predicted colours.

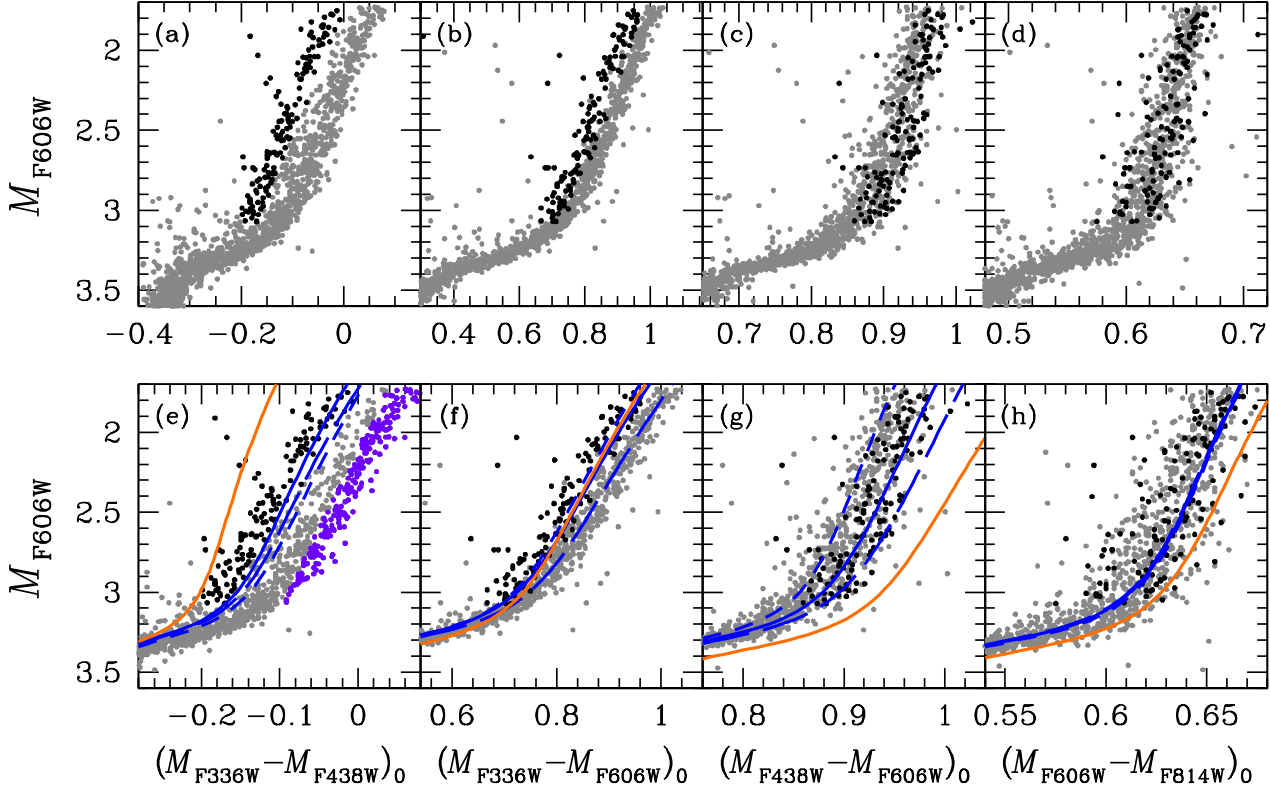


**Figure 8.** Panels (a)–(d): Magnified view of the observed subgiant and lower RGB stars in M5 from the previous figure. The stars represented by filled circles in black were selected on the basis of their  $(M_{F336W} - M_{F438W})_0$  colours (left-hand panel), where they are clearly separated from the redder giants. The locations of the same stars in the other three CMDs are similarly represented by black filled circles. Panels (e)–(h): the same CMDs from the top row are superimposed by the lower RGB portions of isochrones for the a4x0\_p2, a4xC\_p4, and a4xC0 mixtures (the dashed, solid, and long-dashed loci in blue, respectively), along with an isochrone for the a4s08C1 mix (see the text) in orange. All of the isochrones assume  $[\text{Fe}/\text{H}] = -1.33$ ,  $Y = 0.30$ , and an age of 11.4 Gyr. The stars that appear as purple points in panel (e) are discussed in the text.

that would mainly affect their  $T_{\text{eff}}$  and colour zero points. Another caveat is that the observed colour spread is probably affected to some extent by photometric errors.)

The C abundance variations that we have considered apparently do not affect  $M_{F606W} - M_{F814W}$  colours (Fig. 8h), though they may account for a large fraction of the observed spread in the  $M_{F336W} - M_{F606W}$  colours along the lower RGB at a fixed magnitude (see panel f). Unfortunately, the models do not predict sufficiently blue  $M_{F336W} - M_{F438}$  colours to match the stars plotted as black filled circles in panel (e). However, it is interesting that the models for the a4xC\_p4 mix are bluer than those for the a4xC0 mixture, despite having a lower C abundance by 0.3 dex. Since they also have a lower O abundance by 0.2 dex, one cannot help but wonder if the bluest giants in Fig. 8e have high C and low O abundances. (We noted in Paper I that, although the  $F336W$  passband contains an NH band and is therefore sensitive to the abundance of nitrogen, OH is also quite prominent, and there are even some CN features in the reddest part of this passband.) We did not anticipate this possibility when the project began; consequently, models for high C, low O mixtures were not generated. However, we did produce one set of models, mostly for academic interest at the time, that may have some relevance for our present discussion.

This set, which will henceforth be referred to as the “a4s08C1” models, was calculated for the same metal abundances as those listed for the a4s08 mix in Table 1, except that a higher C abundance by 1 dex was assumed. In contrast with the enhanced C mixtures discussed so far, such a large enhancement means that  $C > O$ , which has huge implications for low-T opacities (see Ferguson & Dotter 2008) and synthetic spectra (e.g., Van Eck et al. 2017, see their Fig. 2). Stars with  $C > O$  are predicted to have inflated atmospheres, lower photospheric pressures, and cooler  $T_{\text{eff}}$ s, especially along the RGB. Furthermore, the colours of C-rich stars are very different as a consequence of replacing oxides by polyatomic molecules involving carbon that produce enormous numbers of lines. Plotted as orange curves in Fig. 8 are 11.4 Gyr isochrones for  $[\text{Fe}/\text{H}] = -1.33$ ,  $Y = 0.30$ , and the a4s08C1 mixture of the metals. These models clearly predict much bluer  $M_{F336W} - M_{F438W}$  colours, and much redder  $M_{F438W} - M_{F606W}$  colours, than those of the cluster giants. (The redward offset of the orange curve in panel (h) is due to the effects of  $C > O$  on the model temperatures rather than on the BCs for the  $F606W$  and  $F814W$  filters.) Although such extreme C abundances are not relevant to M5 (or any other GC), there are presumably some combinations of the C and O (and possibly N) abundances for which isochrones will match the observed colours of the giants that lie between the orange and blue loci in Fig. 8e. Explorations similar to those presented here will need to be carried out to determine what mixtures of C, N, and O can provide viable explanations of those stars. Nevertheless, at this point in time, the possibility that M5 contains a population of C-enhanced stars warrants serious consideration.

Even though the MARCS spectra were not extended sufficiently far into the UV to predict BCs for the  $F275$  filter, we were curious to know where the putative C-enhanced stars are located in a CMD in which the  $M_{F275W} - M_{F336W}$  colour is used as the abscissa. It turns out that, as illustrated by the filled black circles in Figure 9, they are the reddest stars in such a CMD, which indicates that they are O-rich. (Since the  $F275W$  passband contains spectral features due to OH, stars with high O abundances will have stronger OH, fainter  $F275W$  magnitudes, and therefore redder  $M_{F275W} - M_{F336W}$  colours.) Moreover, they are clearly separated from the high N, CN-strong population that has the reddest  $(M_{F336W} - M_{F438W})_0$  colours; note that the stars plotted as pur-

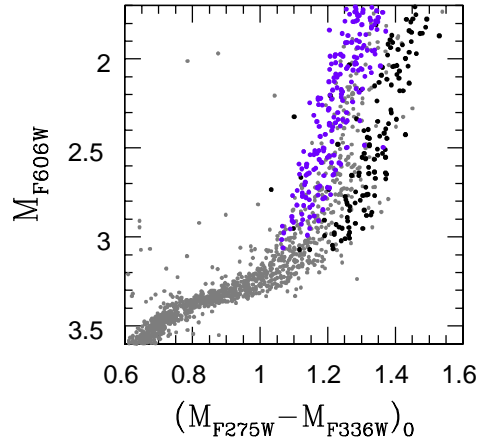


**Figure 9.** As in the previous figure, except that the  $(M_{F275W} - M_{F336W})_0$  colours of the lower RGB stars in M5 have been plotted. The stars represented by black and purple filled circles are the same ones that are similarly identified in Fig. 8e.

ple filled circles are the same ones that are similarly identified in Fig. 8e. These stars apparently have lower O abundances than those shown as black filled circles, which is consistent with expectations, since the highest N abundances will be found in a gas that has undergone ON-cycling. Thus, variations in the efficiency of ON-cycling would provide a natural explanation for the spread in the  $M_{F275W} - M_{F336W}$  colours that is displayed by the purple points in Fig. 9. As fully appreciated by Piotto et al. (2015),  $F275W$  observations clearly provide a very valuable additional constraint on GC abundances. Unfortunately, we do not have the capability to predict the locations of isochrones for different C, N, and O abundances in Fig. 9 due to the limitations of our current models. It would be especially interesting to know where isochrones for  $[\text{O}/\text{Fe}] = 0.6$  are located in this figure.

Some additional features of Fig. 7 are worth pointing out. In contrast with NGC 6362, most of the  $\delta X$  colour offsets are positive; i.e., the isochrones had to be shifted to redder colours in order to match the cluster TOs. Smaller adjustments would have been found had we used isochrones for a higher  $[\text{Fe}/\text{H}]$  value, but we found that, in this case, the models do not fit either the lower RGB or the MS stars nearly as well. (Note that the isochrones for  $[\text{Fe}/\text{H}] = -1.33$  and  $Y = 0.25$  are almost coincident with the median MS fiducial sequences from the SGB down to  $M_{F606W} \sim 5.5$ .) As shown below, fits of isochrones to the CMDs of even more metal-deficient GCs typically require comparable values of  $\delta X$  in order to match the observed TOs.

### 3.4 NGC 5272 (M3)

The basic properties of M3 (NGC 5272) appear to be quite well determined as the result of many investigations over the years. For this system, recent spectroscopic studies have tended to find  $[\text{Fe}/\text{H}]$  values in the range from  $-1.55$  to  $-1.50$  (Kraft & Ivans 2003, Sneden et al. 2004, CBG09), with some preference for the lower, or higher, values if the metallicities are derived from Fe I, or Fe II, lines, respectively. M3 is known to be nearly unreddened; e.g., dust maps yield  $E(B - V) = 0.011 - 0.013$  (Schlegel et al. 1998, Schlafly & Finkbeiner 2011). The latest simulations of the cluster HB population suggest that M3 has a mean He abundance close to  $Y = 0.255$  and a distance corresponding to  $(m - M)_V \approx 15.02$

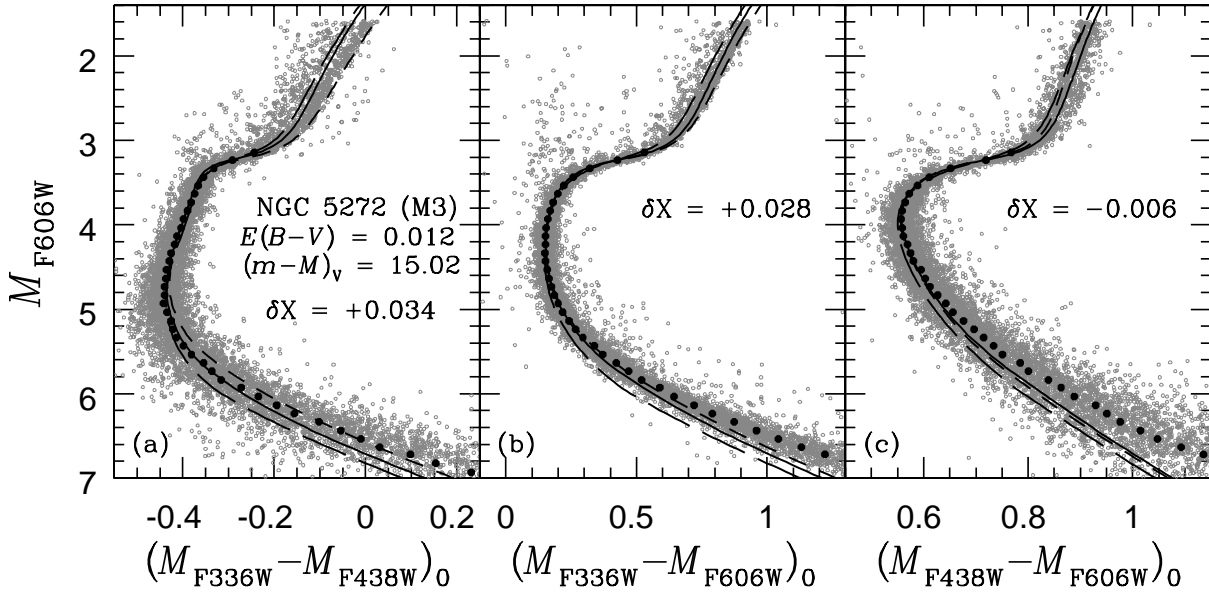


**Figure 10.** Similar to Fig. 7; in this case, WFC3 observations of M3 (from NLP18) have been fitted by a 11.9 Gyr isochrones for  $[\text{Fe}/\text{H}] = -1.55$ ,  $Y = 0.25$ ,  $[\alpha/\text{Fe}] = 0.4$ , and  $[\text{O}/\text{Fe}] = 0.6$ . The long-dashed curve assumes  $Y = 0.30$ . Although the plot is not included here, no colour offsets are needed for the isochrones to match the MS and TO colours on the  $[(M_{F606W} - M_{F814W})_0, M_{F606W}]$  diagram, though the models are too red along the lower RGB by  $\sim 0.03$  mag (as found for all other GCs).

(Denissenkov et al. 2017). Moreover, on the assumption of very similar cluster properties and chemical abundances, stellar models are able to explain the periods of member RR Lyrae variables quite satisfactorily (Vandenberg et al. 2016).

If 11.9 Gyr isochrones for  $[\text{Fe}/\text{H}] = -1.55$ ,  $Y = 0.25$ ,  $[\alpha/\text{Fe}] = 0.4$ , and  $[\text{O}/\text{Fe}] = 0.6$  are fitted to the WFC3 observations of M3, assuming  $E(B-V) = 0.012$  and  $(m-M)_V = 15.02$ , one obtains Figure 10. As in previous plots that contain the same three CMDs, the solid and dashed loci were obtained using the a4x0\_p2 and a4CNN BCs; the long-dashed curve is similar to the solid curve except that it assumes a higher He abundance ( $Y = 0.30$ ). The left-hand panel shows that the isochrones enclose the densest concentration of lower RGB stars without requiring any additional offset to the predicted colours other than the  $\delta X$  value that is needed to fit the TO. However, as in the case of NGC 6362 and M5, a substantial fraction of the giants are distributed to much bluer colours than those predicted by the isochrones at  $M_{F606W} \lesssim 2.8$ . As shown by the long-dashed curve, models for a helium abundance as high as  $Y = 0.30$ , which is well outside the range in  $Y$  that has been derived from simulations of the HB population in M3 (Denissenkov et al. 2017), is incapable of explaining the CMD locations of the majority of the anomalously blue giants.

Interestingly, the M3 giants that lie to the left of the isochrones in Fig 10a have considerably more overlap with the rest of the lower RGB stars (those plotted in gray) on the other CMDs than in the case of M5 (or NGC 6362). This is readily seen by comparing the CMDs in the top row of Fig. 8 for M5 with those shown in top row of Figure 11, which similarly plots just the subgiant and giant-branch stars of M3. Most of the anomalous giants, which are identified by black filled circles, have redder  $(M_{F438W} - M_{F606W})_0$  colours than those predicted by the reddest isochrone in Fig. 10c; the RGB portion of this isochrone has been reproduced as the solid curve (in cyan) in Fig. 11c. Thus, the majority of the stars that are represented by black points show the photometric signature of enhanced C abundances in that they have quite red CMD locations in

panel (c) and moderately blue locations in panel (a), which is the expected consequence of having fainter  $M_{F438W}$  magnitudes when CH and CN bands are stronger.

The TO-to-RGB portions of a few isochrones have been plotted in Figs. 11a–d. The solid curve in blue represents an isochrone for the a40NN mixture to illustrate the predicted colours for a metal abundance mixture with  $[\text{N}/\text{Fe}] \sim 1.5$  and very low abundances of C and O ( $[\text{C}/\text{Fe}] = -0.8$ ,  $[\text{O}/\text{Fe}] = -0.4$ ; see Table 1). This isochrone matches the red edge of the CMD that appears in panels (a), which is the expected consequence of high N and the increased blanketing due to NH in the  $F336W$  passband. This isochrone also lies close to the blue edge of the distribution of lower RGB stars in panel (c), which could have been anticipated because the  $F438W$  filter contains spectral features due to CN (which will be weak) and CH, implying brighter  $F438W$  magnitudes and bluer  $(M_{F438W} - M_{F606W})_0$  colours. (It cannot be concluded from these models that M3 necessarily has stars with such low C abundances because isochrones for the a4CNN mixture, which has  $[\text{C}/\text{Fe}] = -0.3$ , provide very similar fits to the bluest giants; see Fig. 10c and our results for M5 in Fig. 8g. Furthermore, the absolute locations of the isochrones will be affected by whatever errors are present in the BCs and the model  $T_{\text{eff}}$ . The models should be more trustworthy in a relative sense, though the extent of photometric errors remains a concern.)

Not unexpectedly, C-rich stellar models predict very red  $(M_{F438W} - M_{F606W})_0$  colours. As shown by the dashed curve in blue, isochrones for  $Y = 0.30$  and the a4x0 mixture reproduce the location of reddest giants in panel (c) rather well (just as we found in the case of M5; see Fig. 8c). Of course, the same fit to the observations could be obtained using stellar models for a somewhat lower He abundance, provided that a suitably reduced value of  $[\text{C}/\text{Fe}]$  is also assumed, but this could hardly lead to a reduction in the inferred value of  $[\text{C}/\text{Fe}]$  by more than  $\sim 0.2$  dex. Encouragingly, the solid and dashed loci encompass all of the lower RGB stars of M3 on this particular CMD. With regard to panels (a) and (b): al-

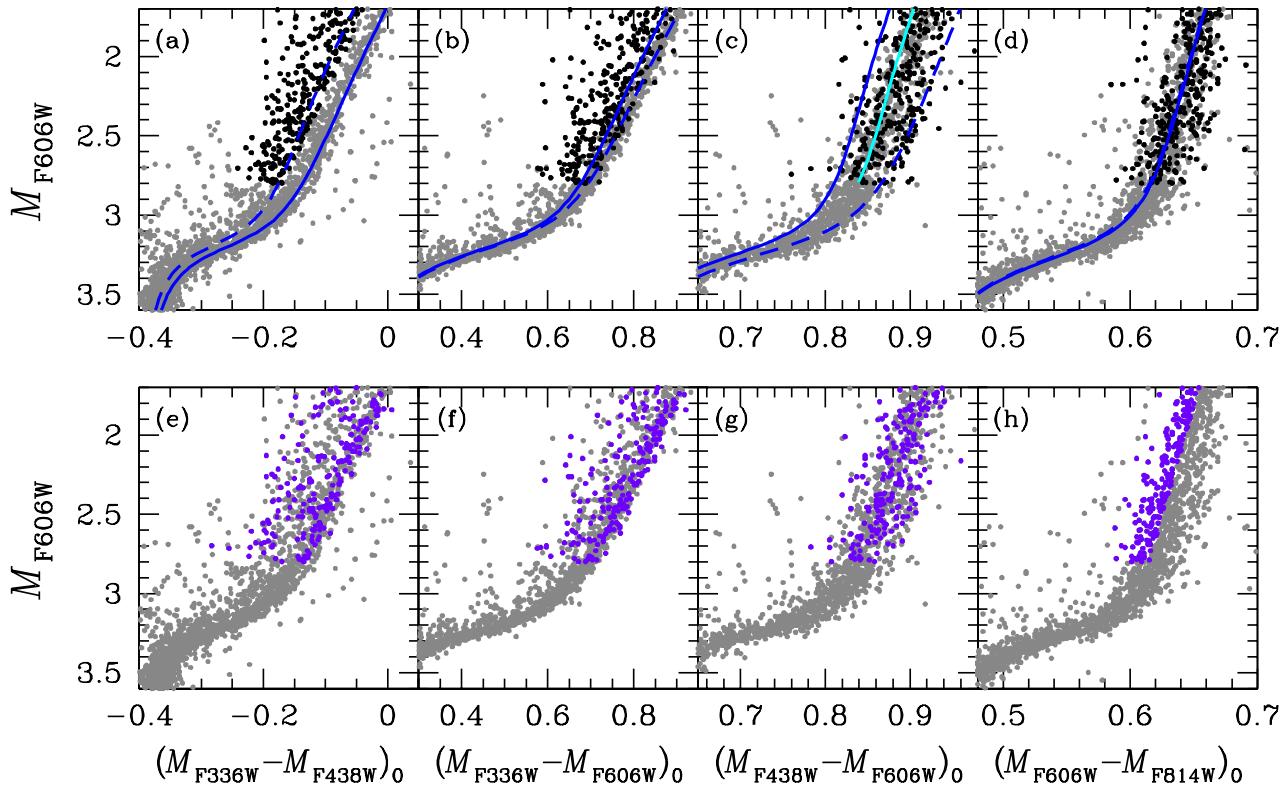


**Figure 11.** Similar to Fig. 8; in this case, expanded views of the subgiant and lower RGB populations of M3 are shown. *Panels (a)–(d)*: the locations of the stars that were selected in panel (a) are plotted as black filled circles in all four CMDs. The nearly vertical line in cyan represents the lower RGB portion of the same isochrone (for the a4CNN mixture) that appears in panel (c) of the previous figure; this is the reddest of the three isochrones that are plotted therein. The isochrones in blue assume the same age (11.9 Gyr) and  $[\text{Fe}/\text{H}]$  value ( $-1.55$ ), but a higher  $Y$  (0.30) and the a40NN and a4xCO mixtures of the metals (solid and dashed loci, respectively). *Panels (e)–(h)*: the locations of the stars that were selected in panel (h) are plotted as purple filled circles in all four CMDs.

though the a4xCO models may be relevant to the reddest of the stars that are plotted as black filled circles, the chemical properties of the bluest of those stars remain a mystery. None of our computations for any of the mixtures of the metals in Table 1 predict such blue colours.

Recall from Paper I (specifically Fig. 5) that high O by itself has the effect of producing redder  $M_{F336W} - M_{F438W}$  colours (due to the effects of enhanced OH). Reduced O abundances would have the opposite effect, but we expect that lower O would be accompanied by higher N, which would drive stars to the red side of the RGB because the BCs for the  $F336W$  filter are more sensitive to NH than to OH. The same can be said about low C, which is normally transformed to N via the CN-cycle. Although the  $F336W$  passband contains some CN features, the BCs for this filter are much more dependent on NH and therefore on the abundance of nitrogen. Since high N causes red  $M_{F336W} - M_{F438W}$  colours, only low N remains as a possible explanation of the bluest stars (if colours are mostly due to variations in the abundances of C, N, and/or O). It would not be too surprising, in fact, if this colour is correlated with the abundance of N from the blue to the red side of the CMD just as the  $M_{F438W} - M_{F606W}$  colour index appears to be directly correlated with C abundances.)

The problem is that we do not expect to find stars with very low N abundances because CN- and ON-cycling always works in the direction of increasing N, and it has generally been found that, as expected for H-burning reactions,  $\text{C} + \text{N} + \text{O} = \text{constant}$  to within measuring uncertainties ( $\delta \log(\text{C} + \text{M} + \text{O}) \sim 0.1$ –

0.15 dex), see, e.g., Smith et al. (1996), Cohen & Meléndez (2005), Carretta et al. (2005). Nevertheless, observations indicate that there are significant populations of stars in GCs with  $0.0 < [\text{N}/\text{Fe}] \lesssim -1.0$ , with some indication that the number of such stars varies inversely with the cluster metallicity (see Cohen et al. 2005, their Figs. 7, 8, 10, and 11). At the present time, large ( $\gtrsim 0.4$  dex) star-to-star variations in  $[\text{CNO}/\text{Fe}]$  have been found in only a few systems that show the strongest evidence for multiple stellar populations — notably, NGC 1851 (Yong et al. 2009), M 22 (Marino et al. 2012b), and  $\omega$  Cen (Marino et al. 2012a). It is possible that smaller variations are present in other systems, perhaps preferentially in the most massive GCs. However, it is not known whether stars with very low N abundances have the same  $\text{C} + \text{N} + \text{O}$  abundance as cluster members with  $[\text{N}/\text{Fe}] \gtrsim 0.0$ . This should be checked.

The answer to another question remains elusive: what is the origin of the relatively large spread in the  $(M_{F606W} - M_{F814W})_0$  colour at a fixed magnitude along the lower RGB? The  $F606W$  and  $F814W$  filters are mainly sensitive to CN (see, e.g., Sbordone et al. 2011, their Fig. 4), but at low metallicities and assuming normal abundances of C and N, CN is not sufficiently important to affect  $M_{F606W} - M_{F814W}$  colours by more than  $\sim 0.005$  mag (see the  $\delta(\text{BC})$  plots shown in Fig. 5 of Paper I). To be sure, the effects are larger than this at higher  $[\text{Fe}/\text{H}]$  values; recall Fig. 1c, which showed that CN-strong giants in 47 Tuc will be  $\sim 0.015$  mag bluer than its CN-weak counterparts at the same  $M_{F606W}$ . (Similar results were obtained by Milone et al. 2018.) The difficulty with CN is that the effects on BCs will diminish rapidly with decreas-

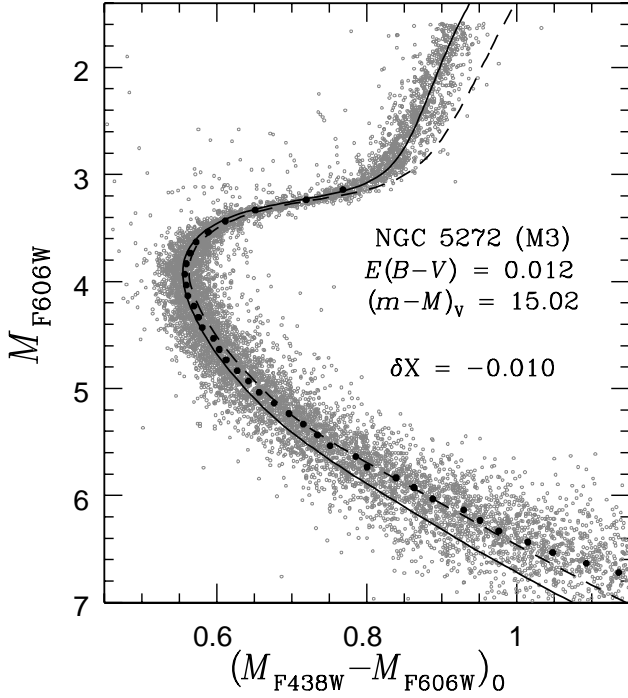


**Figure 12.** Similar to Fig. 10c, except that the location of an isochrone for the a4xCO mixture (dashed curve) has been fitted to the CMD of M3 along with one for the a4x0\_p2 mix.

ing metallicity because the abundances of both C and N will be reduced at lower  $[\text{Fe}/\text{H}]$  values, and hence the effect on CN-band strengths will be quadratic. (For the same reason  $F336W$  magnitudes will be more sensitive to NH, and  $F438W$  magnitudes to CH, than to CN bands, at low metallicities.) It would therefore seem to be necessary to have much higher abundances of C and N than in the standard a4s21 and a4CNN mixtures if CN is responsible for the bluest  $M_{F606W} - M_{M814W}$  colours at the low  $[\text{Fe}/\text{H}]$  values.

Helium abundance variations would seem to be the only other way of inducing large spreads in the  $M_{F606W} - M_{F814W}$  colour. An important advantage of such variations is that their effects on this particular colour index would be similar for different  $[\text{Fe}/\text{H}]$  values. Other colours are affected much more by variations in C, N, and O than He abundance differences. For instance, as discussed just above, the reddest giants in M3 would appear to have quite high C, irrespective of whether they have enhanced He abundances. The bottom row of panels in Fig. 11 shows that the bluest giants in panel (h), where they are identified by purple points, are not at all isolated to particular colour ranges in the CMDs shown in panels (e), (f), and (g), but instead span the entire colour ranges of the respective CMDs. In other words, stars with apparently wide variations in the abundances of C and N, have very similar  $M_{F606W} - M_{V814W}$  colours. According to, e.g., Cohen et al. (2005, their Figs. 10 and 11), the star-to-star variations of  $[\text{C}/\text{Fe}]$  and  $[\text{N}/\text{Fe}]$  within GCs range from 0.8 to 1.3 dex and 1.7 to 2.8 dex, respectively. Note, as well, that small fractions of the stars in some of the clusters that they considered appear to have  $[\text{C}/\text{Fe}] \sim 0.2$ – $0.3$  and  $[\text{N}/\text{Fe}] \gtrsim 1.7^4$  (also see Briley et al. 2004). It is tempting to conclude that helium is primarily responsible for the variation in

<sup>4</sup> These results assume solar abundances that are about 0.2 dex higher than those determined subsequently by Asplund et al. (2009); consequently, the

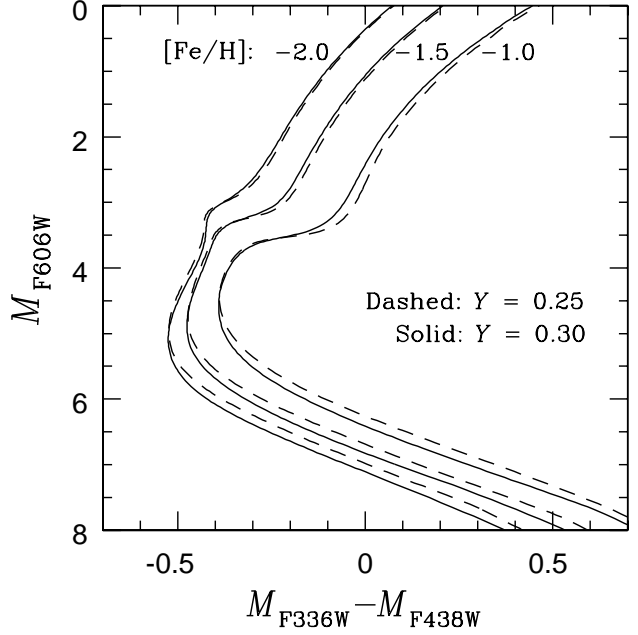


**Figure 13.** Comparisons of 12.5 Gyr isochrones for  $[\alpha/\text{Fe}] = 0.4$  and  $[\text{Fe}/\text{H}] = -2.0, -1.5,$  and  $-1.0$  assuming, for each metallicity,  $Y = 0.25$  and  $0.30$  (as indicated).

the observed  $M_{F606W} - M_{F814W}$  colour along the lower RGB, and that CN plays a secondary role.

The MS of M3 also seems to be somewhat anomalous in that its slope in Fig. 10c is much shallower than that predicted by our isochrones for the a4x0\_p2 mixture. Such a strong deviation between the models and the observations, which begins at  $M_{F606W} \approx 4.5$ , was not seen in the GC CMDs considered thusfar. Furthermore, the spread in the  $(M_{F438W} - M_{F606W})_0$  colours at a given magnitude seems unusually large, which gives one the distinct impression that  $F438W$  magnitudes are more problematic than either those for the  $F336W$  or  $F606W$  passbands. While it would not be surprising that there would be systematic errors in any of the colours with increasing  $F606W$  magnitude along the MS (due, e.g., to problems with the predicted temperatures of stellar models or systematic errors in the BCs that are correlated with the temperatures or colours of stars), the large morphological differences may be another indication that some stars in M3 have unusually high C abundances. In fact, the MS slope on the  $(M_{F438W} - M_{F606W})_0$   $M_{F606W}$  CMD is predicted to be a function of the C abundance. This is illustrated in Figure 12, which shows that isochrones for the a4xCO mixture provide a much better fit to the MS fiducial of M3 than the a4x0\_p2 models.

We searched for other explanations, but unsuccessfully. For instance, we generated grids of evolutionary tracks and isochrones for alternative values of  $[\text{Fe}/\text{H}]$  (between  $-1.6$  and  $-1.45$ ), and for reduced O abundances by 0.2 dex, without finding a significant change to the predicted slope of the MS. (Higher  $Y$  exacerbates the problem.) We also ruled out the possibility that interpolation errors in the relevant  $\delta(\text{BC})$ – $\log g$  relations (like those plotted in Fig. 2 of Paper I) are responsible for the shallow MS slope, but essentially the same slope is predicted by the CV14 transformations. It would

reported values of  $[\text{C}/\text{Fe}]$  and  $[\text{N}/\text{Fe}]$  should be increased by 0.2 dex to put them on the Asplund et al. scale.

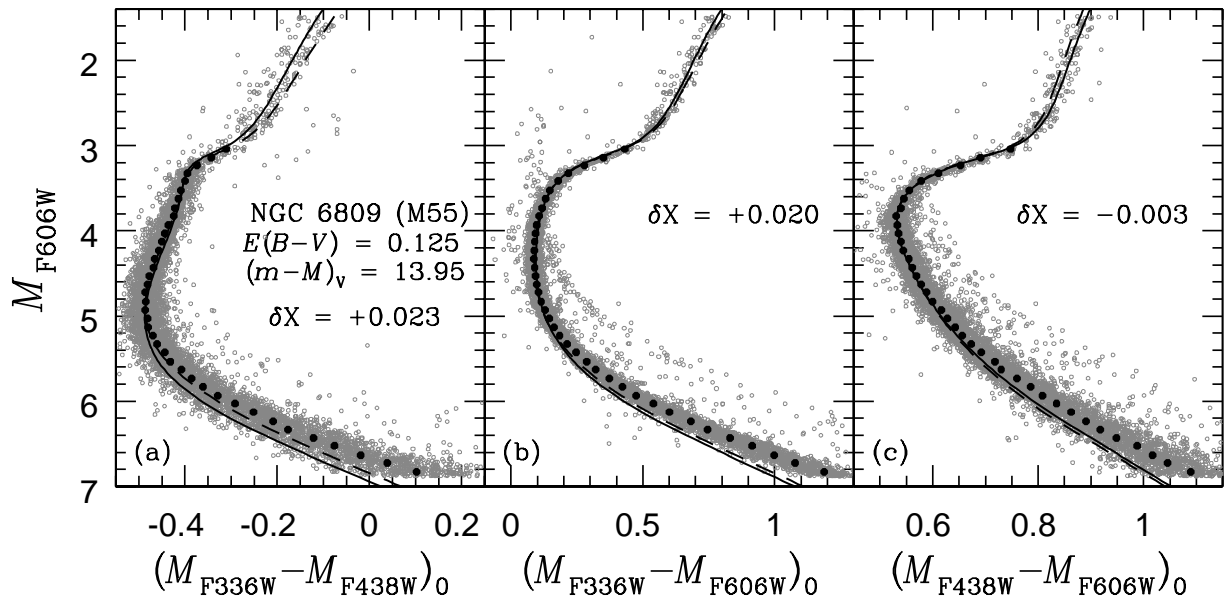


**Figure 14.** Similar to Fig. 10; in this case, WFC3 observations of M 55 (from NLP18) have been fitted by 12.8 Gyr isochrones for  $[\text{Fe}/\text{H}] = -1.93$ ,  $\langle Y_0 \rangle = 0.265$ ,  $[\alpha/\text{Fe}] = 0.4$ , and  $[\text{O}/\text{Fe}] = 0.6$ . Fits to  $F606W$ ,  $F814W$  photometry (not shown) are very similar to those obtained for other GCs; i.e., the isochrones require only a small offset in the predicted colours ( $-0.006$  mag) to match the MS and TO observations, but their lower RGB portions are too red by  $\sim 0.03$  mag.

therefore appear that enhanced C abundances are favoured by both the observed MS slopes and the fits of isochrones to GC giants with the reddest  $M_{F438W} - M_{F606W}$  colours; i.e., the assumption that GC stars have  $[\text{C}/\text{Fe}] \lesssim 0.0$  may not be correct. Although such results as those shown in Fig. 10 seem quite agreeable, at least in an overall sense, we suspect that it could be quite fruitful to explore the consequences of wider variations in the abundances of C and N than in our current models.

As regards the small discrepancies at  $M_{F606W} \sim 5.4$  in Fig. 10a, they can be reduced by adopting a lower metallicity or a higher He abundance. Consider Figure 13, which shows that the magnitude difference between the roughly horizontal transition from the TO to the RGB at  $M_{F606W} \lesssim 3.5$  and the MS at  $M_{F606W} \gtrsim 5.8$  varies inversely with  $[\text{Fe}/\text{H}]$  (and age) and directly with  $Y$ . The morphology of an isochrone in the vicinity of the TO is also quite a strong function of the metallicity — much more so than in optical CMDs. Indeed, the location and shape of the principal photometric sequence of M 3 on the  $[m_{F336W} - m_{F438W}, m_{F606W}]$ -diagram provides a compelling argument that this cluster has a metallicity within  $\pm 0.1$  dex of  $[\text{Fe}/\text{H}] = -1.55$ . Curiously, isochrones for the same  $[\text{Fe}/\text{H}]$  value and age are predicted to be slightly redder at the TO ( $M_{F606W} \sim 4.0$ ) if they assume a higher  $Y$ , which is contrary to expectations given that the turnoff  $T_{\text{eff}}$  is predicted to be somewhat hotter (by 20–40 K) if  $Y = 0.30$  than if  $Y = 0.25$ . The same behavior is, however, found if the CV14 transformations are used to transpose the models from the theoretical to the observed plane.

The  $\delta X$  colour offsets in Fig. 10 are somewhat smaller than those determined for M 5, but in the same sense. As in the latter cluster, they suggest that the predicted  $M_{F336W}$  magnitudes near the TO are slightly too bright. These offsets would be reduced if a higher metallicity were adopted, but doing so would increase the discrepancy between the predicted and observed  $M_{F438W} - M_{F606W}$  colours. Moreover, models for a higher  $[\text{Fe}/\text{H}]$  value would not be able to match the CMD locations of either the lower RGB stars or the MS stars at  $M_{F606W} \sim 5.5$  quite as well. If any-

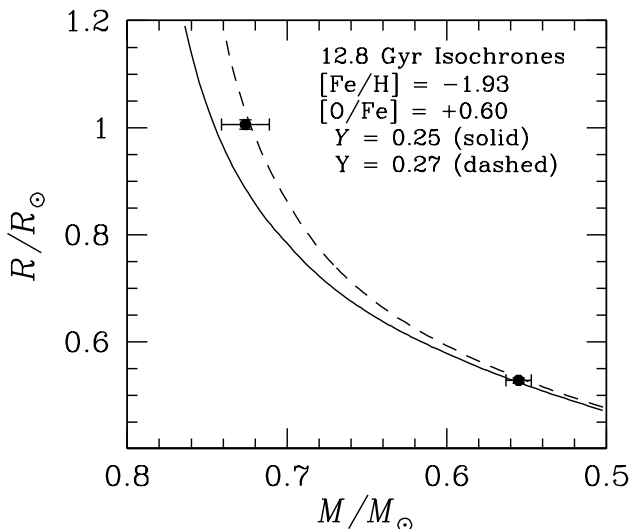


**Figure 15.** Mass-radius relations from 12.8 Gyr isochrones for  $[\text{Fe}/\text{H}] = -1.93$  and the indicated values of  $[\text{O}/\text{Fe}]$  and  $Y$  are compared with the properties of the binary V54 (filled circles and error bars) that were derived by Kaluzny et al. (2014).

thing, these observations suggest that M 3 may have a slightly lower metallicity (closer to  $[\text{Fe}/\text{H}] = -1.6$ ).

### 3.5 NGC 6809 (M 55)

In their recent study of M 55, Vandenberg & Denissenkov (2018) concluded from their analysis of its CMD, the cluster RR Lyrae variables, and the eclipsing binary V54 (Kaluzny et al. 2014) that it has a reddening in the range  $0.12 \lesssim E(B-V) \lesssim 0.13$ , as found from dust maps (Schlegel et al. 1998, Schlafly & Finkbeiner 2011),  $(m-M)_V = 13.95 \pm 0.05$ , which was also shown to agree very

well with the distance derived from MS fits to local subdwarfs,  $[\text{Fe}/\text{H}] = -1.85 \pm 0.1$ , in agreement with spectroscopic findings (e.g., CBG09), and  $[\text{O}/\text{Fe}] = 0.5 \pm 0.1$ . Furthermore, the simulations of the cluster HB populations that were presented in the same investigation indicated that most of the core He-burning stars have  $0.25 \lesssim Y_0 \lesssim 0.27$  with only  $\sim 10\%$  of them having slightly higher He abundances. In keeping with our analyses of M 3 and M 5, we have adopted the metallicity given by Carretta et al. ( $-1.93$  to be specific),  $[\text{O}/\text{Fe}] = 0.6$  (with  $[m/\text{Fe}] = 0.4$  for the other  $\alpha$  elements), and the aforementioned cluster parameters. Under these assumptions, 12.8 Gyr isochrones for approximately the mean He abundance,  $\langle Y_0 \rangle = 0.265$ , provides reasonably good fits to the WFC3 CMDs for M 55 — as shown in Figure 14 — when they are transformed to the observational planes using the a4x0 and a4CNN BCs.

The left-hand panel, in particular, provides strong support for the adopted  $[\text{Fe}/\text{H}]$  value given that the morphology of the  $[(M_{F336W} - M_{F438W})_0, M_{F606W}]$ -diagram depends quite sensitively on metallicity (recall our discussion of Fig. 13). The separation of the solid and dashed loci along the lower RGB is also quite a strong inverse function of  $[\text{Fe}/\text{H}]$ ; compare these predictions with those applicable to M 3 in Fig. 10 and NGC 6362 in Fig. 5. As for all of the other GCs considered in this study, none of our stellar models is able to reproduce the CMD locations of the bluest, lower RGB stars, though we suspect that at least some of the giants may have relatively low N abundances. On the other hand, at very low metallicities in particular, colours are only weakly dependent on the abundances of the light elements and it seems doubtful that stellar models for reduced N by 0.5–0.7 dex or so would predict the relatively large variation in the  $(M_{F336W} - M_{F438W})_0$  colours at a given  $M_{F606W}$  to the left of the solid curve in Fig. 14a, which assumes  $[\text{N}/\text{Fe}] = 0.0$ . Perhaps something other than metal abundance variations is responsible for the relatively large width of the lower RGB of M 55 in this panel.

Aside from this difficulty and the usual deviations between the predicted and observed MS slopes, the models provide satisfactory fits to the WFC3 photometry. Note that the  $\delta X$  offsets are slightly less than, though similar to, those found for M 3. Finally, given the importance of the binary constraint, we show in Figure 15 that the mass-radius relations from the isochrones for the same metal abundances, but for He abundances that have been inferred from HB simulations (VandenBerg & Denissenkov 2018), are consistent with the masses and radii that have been determined for the eclipsing binary member, V54, by Kaluzny et al. (2014).

### 3.6 NGC 6341 (M 92)

M 92 is a suitable representative of the most metal-deficient GCs in the Milky Way given that it is subject to relatively low reddening ( $E(B - V) = 0.019 - 0.023$  according to the dust maps of Schlegel et al. 1998 and Schlafly & Finkbeiner 2011), most determinations of its apparent distance modulus lie in the range  $14.65 \leq (m - M)_V \leq 14.79$  (see the summary of published results given by VandenBerg & Denissenkov 2018, their Table 1), and spectroscopic studies generally find  $[\text{Fe}/\text{H}] \sim -2.35$  (Kraft & Ivans 2003, CBG09). However, a significantly lower metallicity,  $[\text{Fe}/\text{H}] \lesssim -2.6$ , has been recently derived by Roederer & Sneden (2011); consequently, the metal abundance of M 92 may be the least well determined of its basic properties. Nevertheless, if we adopt  $[\text{Fe}/\text{H}] = -2.35$  (from CBG09) and the same values of  $\langle Y_0 \rangle$ ,  $[\alpha/\text{Fe}]$ , and  $[\text{O}/\text{Fe}]$  that were adopted for M 55, which has a very similar HB morphology, we obtain the fits of 12.6 Gyr isochrones to the WFC3 photometry of M 92 that are shown in panels (a) to (c) of Fig-

ure 16. These results assume  $E(B - V) = 0.023$  and  $(m - M)_V = 14.72$ , which are supported by the fits of ZAHB models to the lower boundary of the distribution of cluster HB stars (see, e.g., VBLC13).

Although the distinctive hook feature at  $M_{F606W} \sim 3.1$  in the top, left-hand panel is reproduced very well by the models, it is somewhat disconcerting that rather large  $\delta X$  colour offsets are needed in Figs. 16a and 16b in order to register the isochrones to the observed TOs. The fact that the isochrones need to be shifted to redder colours possibly suggests that the adopted metallicity is too low, which is also indicated by the differences between the isochrones and the median fiducial sequence at  $M_{F606W} \gtrsim 5.2$  in the left-hand panel. Not only would a lower metallicity increase these discrepancies along the lower MS, but larger colour offsets (though only by small amounts) would also be needed in order for the isochrones to match the TO and MS observations because isochrones for lower  $[\text{Fe}/\text{H}]$  values are bluer.

On the other hand, if the metallicity given by CBG09 is increased by 0.15 dex to  $[\text{Fe}/\text{H}] = -2.2$ , one obtains remarkably good fits to the MS and TO observations of M 92; see Figs 16d–f. These results appear to preclude the very low metallicity that was derived by Roederer & Sneden (2011). Apparently, the  $\delta X$  offsets are not very dependent on the assumed  $[\text{Fe}/\text{H}]$  value, as they are still quite large even if M 92 has  $[\text{Fe}/\text{H}] = -2.2$ . At such low  $[\text{Fe}/\text{H}]$  values, variations in the mixture of the metals should have almost no effects on the predicted colours (see Paper I), so the large colour offsets may be due, at least in part, to problems with the BCs or the model  $T_{\text{eff}}$  scale. Alternatively, M 92 may have a higher reddening than we have assumed, as suggested by King et al. (1998). Since  $E(F336W - F606W) = 2.26 E(B - V)$  (see CV14), an increased reddening by only 0.01 mag would reduce the discrepancy between the predicted and observed  $(M_{F336W} - M_{F606W})_0$  colours by 0.026 mag (i.e., by slightly more than a factor of two).

Perhaps the main difficulty with Figs. 16 is that the models are unusually red along the giant branch. Unlike M 55, M 3, and M 5, there are very few stars with redder  $(M_{F438W} - M_{F606W})_0$  colours than the isochrones (see panels c and f). This could be suggesting that M 92 stars have lower C abundances than those residing in the other three GCs, but with so many uncertain factors at play in the fits of isochrones to observed CMDs, the correct explanation could easily be something else. In fact, better consistency in this regard would be obtained if M 92 has  $[\text{Fe}/\text{H}] \lesssim -2.5$  (as derived by Roederer & Sneden 2011), since the lower RGB portions of isochrones for such low metallicities are significantly bluer than those shown in Fig. 16. However, in this case, the models would not match the MS fiducial at  $M_{F606W} \gtrsim 5.2$  nearly as well — though the discrepancies could still be within the uncertainties associated with the assumed distance, the synthetic BCs, and the predicted temperatures.

More than any of the other GCs that we have considered, M 92 raises the concern that photometric errors may be playing a significant role in the observed colour spreads at a given evolutionary stage. According to Paper I, none of the metal abundance variations that we have considered in this project should have any effects on the magnitudes and colours of TO stars at  $[\text{Fe}/\text{H}] \lesssim 2.0$ , and yet the widths of the various CMDs at the TO are  $\gtrsim 0.05$  mag. The only possible “chemical” explanation would seem to be He abundance variations, but our isochrones indicate that the effects of  $\delta Y = 0.04$ , which is probably close to the maximum such variation in M 92, would affect TO colours by no more than 0.01 mag. This leaves photometric scatter as the most likely explanation.

This suggestion is supported by Figure 17. If the M 92 stars

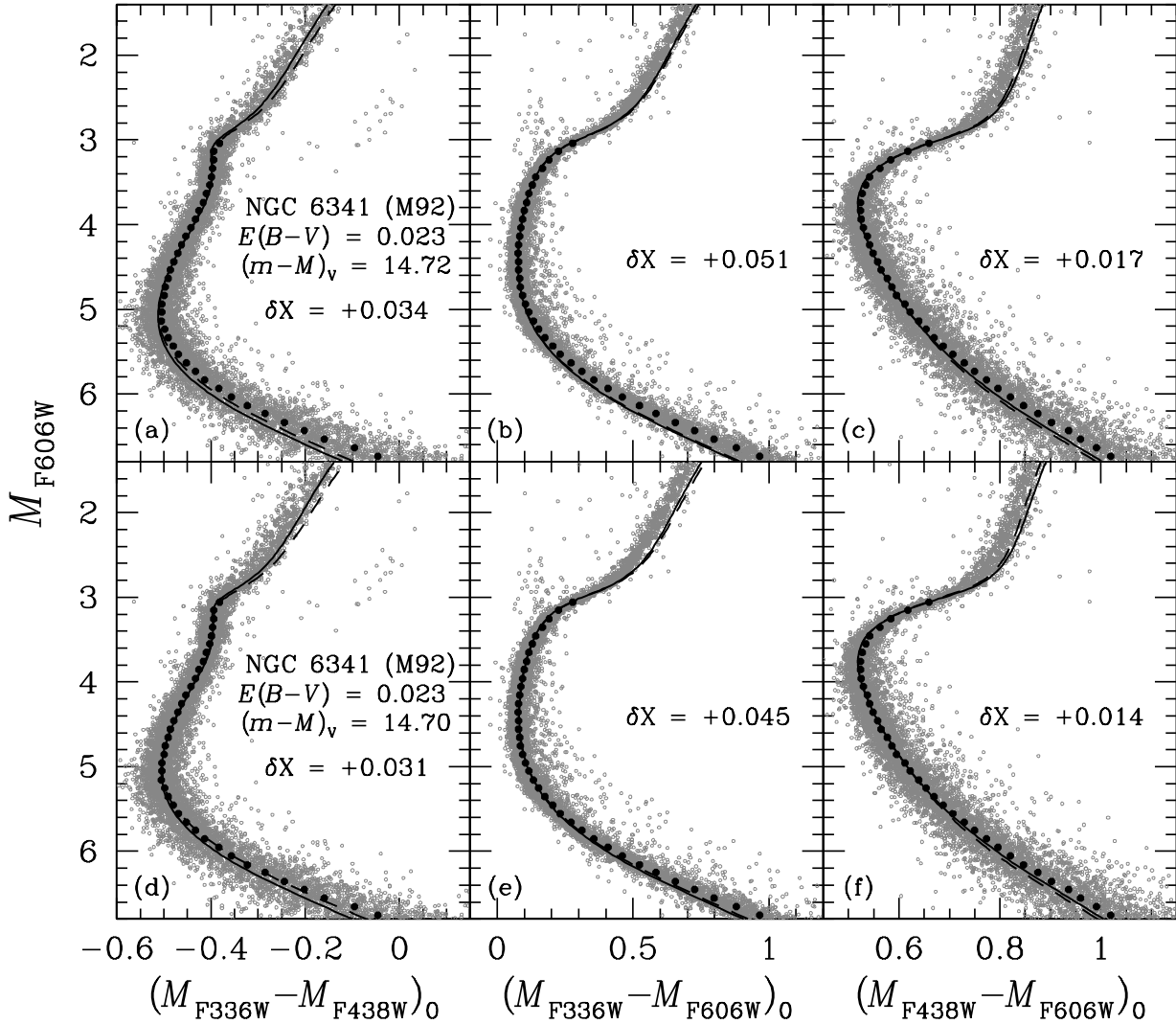


**Figure 16.** Similar to Fig. 10; in this case, panels (a) to (e) show fits of 12.6 Gyr isochrones for  $[\text{Fe}/\text{H}] = -2.35$ ,  $\langle Y_0 \rangle = 0.265$ ,  $[\alpha/\text{Fe}] = 0.4$ , and  $[\text{O}/\text{Fe}] = 0.6$  to WFC3 observations of M92 (from NLLP18). Panels (d) to (f) show similar fits, but using 12.3 Gyr isochrones for  $[\text{Fe}/\text{H}] = -2.20$ . In either of these cases, the isochrones provide very good fits to  $F606W$ ,  $F814W$  observations (not shown) along the upper MS and TO if they are adjusted by  $\delta X \approx -0.004$ , though the predicted giant-branch locations are too red by  $\sim 0.04$  mag. As already mentioned, such fits are common to all of the GCs that we have considered.

with the reddest  $(M_{F606W} - M_{F814W})_0$  colours, at a given  $M_{F606W}$ , have somewhat lower He abundances than those with bluer colours, such stars should also have the reddest  $(M_{F438W} - M_{F606W})_0$  colours (assuming that the colours are not affected by any metal abundance variations that might be present, as predicted by our stellar models for very low metallicities). However, the reddest stars in panel (d), specifically those plotted as black filled circles, which have been constrained to lie within narrow bands, have very wide colour distributions in the other panels. One has the visual impression that the MS distributions in panels (b) and (c) are skewed just slightly to the red, but not by very much. Similarly, if a selection is made in panel (c) of the lower RGB stars with the reddest  $(M_{F438W} - M_{F606W})_0$  colours (e.g., the giants identified by filled circles in purple), they have very broad colour distributions in all of the other CMDs. In fact, stars that have very similar colours in any one of the four CMDs span wide colour ranges in the other three CMDs. The thickness of the principal photometric sequence in M92 is apparently due mostly to photometric errors.

This does not call into question our findings in the case of M5 and M3; specifically the identification of C-rich, N-rich, and O-rich populations in those GCs, because their locations in the various CMDs differ in the expected ways due to the effects of CH and CN on  $F438W$  magnitudes, of NH on  $F336W$  magnitudes, and of OH on  $F275W$  magnitudes. (The absolute abundances of C, N, and O are also much higher in these clusters than in M92, and consequently, spectral features due to molecules that involve atoms of these elements will be much stronger. To a considerable extent, our isochrones are able to explain the observed CMDs.) However, photometric errors may explain the unusually blue colours of some of the cluster giants, since the scatter due to, e.g., the blending of images of pairs or groups of stars will be preferentially to the blue side of the RGB (Bergbusch & Stetson 2009). Complementary spectroscopic studies of samples of the bluest, and the reddest, lower RGB stars with the very best photometry would undoubtedly be very fruitful.

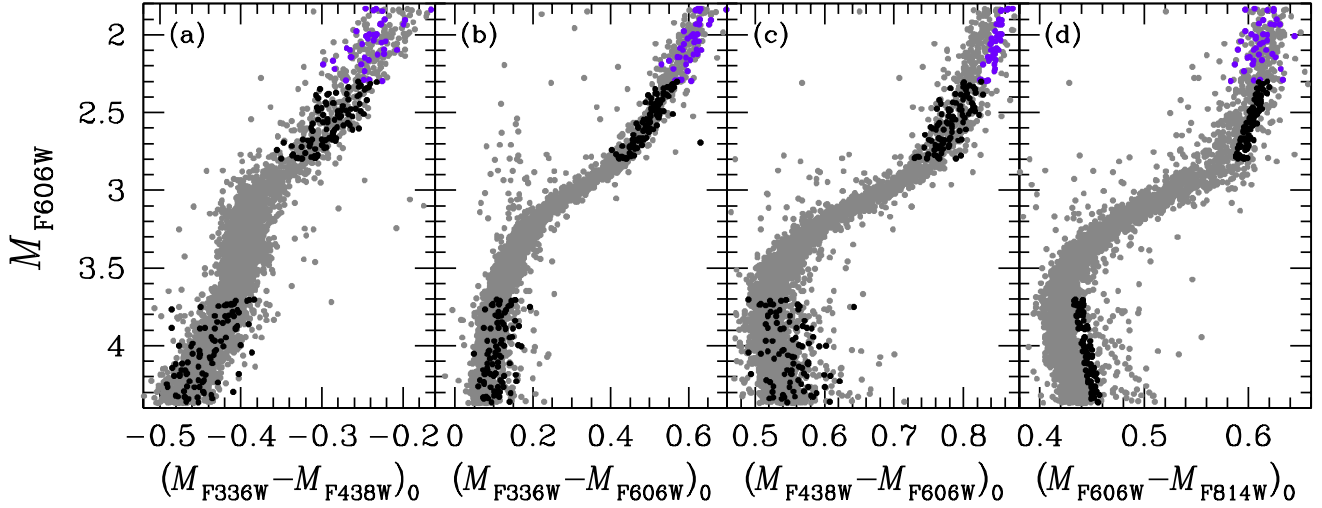


**Figure 17.** Magnified view of the upper MS, TO, and lower RGB portions of the M 92 CMDs. Samples of the giants and upper MS stars that lie within the narrow bands in panel (d), which have the reddest  $(M_{F606W} - M_{F814W})_0$  colours, are plotted in all four panels as black filled circles. Similarly, a selection of the giants in panel (c) with the reddest  $(M_{F438W} - M_{F606W})_0$  colours appear in all four panels as purple filled circles.

#### 4 SUMMARY AND DISCUSSION

This investigation has shown that Victoria-Regina isochrones together with the BCs that have been derived from the latest MARCS model atmospheres and synthetic spectra are able to reproduce the morphologies of the CMDs that can be generated from *HST* UV Legacy Survey WFC3 photometry (Piotto et al. 2015, NLP18) surprisingly well. Even in an absolute sense, the models appear to be able to match observed UV, optical, and near-IR magnitudes and colours to within  $\sim 0.03$  mag, which is easily within the total uncertainty due to possible errors in the  $T_{\text{eff}}$  scale, the zero points of both the synthetic and observed photometry, the adopted cluster properties (i.e., distances, reddening, and metallicities), and remaining deficiencies of the synthetic spectra. Of particular note is the capability of the isochrones to reproduce the development of the “kink” that appears near the TO in  $(M_{F336W} - M_{F438W})_0$ ,  $M_{F606W}$  CMDs at  $[\text{Fe}/\text{H}] \sim -1.8$ , becoming quite a pronounced feature as the metallicity decreases below  $[\text{Fe}/\text{H}] \sim -2.0$ . There is some tendency for the predicted colours to deviate to the blue of observed colors along the LMS, which may be telling us that the assumed carbon abundances are too low, but there are no obvious deficiencies in the fitting of upper MS, TO, and the densest concentrations of lower RGB stars. As shown in Paper I, the improved BCs, especially at UV wavelengths, are superior to those provided by CV14, which are based on the previous generation of MARCS models (Gustafsson et al. 2008), and apparently those derived from Kurucz model atmospheres and synthetic spectra as well (see Martins et al. 2017).

The main thrust of this project has been to examine the consequences of variations in the abundances of C, N, and O for GC CMDs. Our focus has been on lower RGB stars where the effects of light-element abundance variations are predicted to be quite substantial (see Fig. 5 in Paper I). The giant-branch populations of 47 Tuc, NGC 6362, M 5, M 3, M 55, and M 92, which span the range in  $[\text{Fe}/\text{H}]$  from  $\sim -0.7$  to  $\sim -2.3$ , show qualitatively similar morphologies, but with colour spreads that vary with metallicity. The most straightforward CMD to explain seems to be the  $(M_{F438W} - M_{F606W})_0$ ,  $M_{F606W}$  diagram, as the star-to-star colour variation at a given magnitude is predicted to be strongly corre-

lated with the abundance of carbon (in the sense that the C abundance increases in the direction from blue to red). The dependence is unlikely to be strictly linear, however, given the existence of He abundance variations, but carbon has a much greater effect on the  $(M_{F438W} - M_{F606W})_0$  colour than He.

The isochrones that have been fitted to  $F438W$ ,  $F606W$  observations of M 5 and M 3 suggest that some of their stars may have  $[\text{C}/\text{Fe}]$  as high as  $\sim +0.5$  dex. It is difficult to assess the reliability of this prediction because the  $T_{\text{eff}}$ s and colours of stellar models depend on so many factors, each with their own uncertainties, but we note that isochrones for the low C abundances that result from CN- or ON-cycling provide good fits to the blue edges of the colour distributions and that rather high C is needed to obtain comparable fits to the reddest stars. Thus, the observed colour spreads suggest quite a wide range in abundance of carbon. By comparison, field halo stars with high values of  $[\alpha/\text{Fe}]$  have  $[\text{C}/\text{Fe}] \sim 0.2\text{--}0.3$  (Nissen et al. 2014), which is similar to the C abundances that have been derived for GCs by Briley et al. (2004) and Cohen et al. (2005) once their determinations have been adjusted to be on the Asplund et al. (2009) solar scale. It is worth mentioning that the eclipsing binary stars in GCs favor stellar models that assume  $[\text{O}/\text{Fe}] \gtrsim 0.6$  and  $[m/\text{Fe}] \approx 0.4$  for the other  $\alpha$  elements. If  $[\text{O}/\text{Fe}] \lesssim 0.6$  in GCs, as found in solar neighborhood Pop. II stars (Fabbian et al. 2009, Ramírez et al. 2013, Nissen et al. 2014, Amarsi et al. 2019b), then an enhancement in the abundance of carbon would help to satisfy the binary constraint (since the observed  $M$ - $R$  relations for GC binaries seem to require high values of  $[\text{CNO}/\text{Fe}]$ ).

The  $(M_{F336W} - M_{F438W})_0$ ,  $M_{F606W}$  diagram can be used to identify stars with different N abundances (Piotto et al. 2015), and/or C abundance variations since increased C will result in fainter  $M_{F438W}$  magnitudes, and therefore bluer  $(M_{F336W} - M_{F438W})_0$  colours. In the case of GCs, this CMD typically consists of two components — a dense concentration of giants with red colours, and a bluer, usually somewhat more diffuse population that appears to be a separate sequence in clusters with intermediate metallicities (such as NGC 6362 and M 5) or one that overlaps with the reddest stars in lower metallicity systems (e.g., M 3, M 55, M 92). Our isochrones generally provide good fits to the first component, but not the second, if they assume  $[\text{CNO}/\text{Fe}] \approx 0.44$  and

allow for variations in the abundances of C and N that would be produced by CN-cycling. In particular, models for  $[C/Fe] = [N/Fe] = 0.0$ , which are relevant to “CN-weak” stars, and those for  $[C/Fe] = -0.3$  and  $[N/Fe] = 1.13$ , which is representative of the abundances in “CN-strong” stars, contain the observed spreads in the  $(M_{F336W} - M_{F438W})_0$  colours of the redder giants, as well as the metallicity dependence of these spreads, remarkably well.

However, our current models are unable to explain the  $(M_{F336W} - M_{F438W})_0$  colours of the bluer RGB component if they have  $[N/Fe] \geq 0.0$ . As noted in the previous paragraph, isochrones for  $[N/Fe] = 0.0$  coincide with the blue edges of the red RGB populations in GCs, from which one might conclude that the bluest giants must have much lower N abundances. In fact, this would seem to be the only possible “chemical” solution to the puzzle. Although some of our metal abundance mixtures allow for low or high C abundances, and others allow for low or high O abundances, the isochrones for such mixtures are significantly too red (see Figs. 8 and 11). Thus, the very blue  $(M_{F336W} - M_{F438W})_0$  colours cannot be attributed solely to the effects of C and/or O abundance variations on the BCs for the  $F336W$  and/or the  $F438W$  filters. Whether or not weak NH, due to very low N abundances, can explain the bluest  $(M_{F336W} - M_{F438W})_0$  colours remains to be determined as we did not compute any models for low values of  $[N/Fe]$ . However, it is a concern that, at the lowest metallicities, variations in C, N, and O are predicted to have very small effects on colours, even along the lower RGB. It may well turn out that low N is not the answer. Indeed, an explanation of the anomalously blue giants in terms of binaries and evolved blue stragglers may be an especially promising alternative possibility; see Marino et al. (2019).

Regardless, it would still be of considerable interest if GCs contain populations of stars with very low N abundances. Even though it is often assumed that GC stars have  $[N/Fe] = 0.0$  or higher, there have been a number of investigations of metal-deficient field dwarfs over the years that have reported values of  $[N/Fe]$  between  $\sim -0.2$  and  $\sim -0.7$  (e.g., Tomkin & Lambert 1984, Laird 1985, Carbon et al. 1987). Importantly, such stars appear to be present in GCs as well (see Cohen et al. 2005, their Figs. 6, 8, and 10). On the other hand, the reliability of such findings is questionable given that “nitrogen abundances are notoriously difficult to determine with accuracy” (Kraft 1994, p. 57). Some of the causes of this uncertainty are described by Spite et al. (2005), who found, for instance, that there are systematic differences amounting to 0.4 dex between the N abundances that are derived from NH and CN bands. Nevertheless, Spite et al. concluded that the low-luminosity, unmixed giants in their sample of extremely metal-poor stars ( $[Fe/H] < -2.7$ ) have N abundances that extend as low as  $[N/Fe] \sim -1.0$ . They note that such abundances could have been produced by the same Type II supernovae that are believed to be responsible for releasing so much oxygen into the early universe, as suggested by the models of Meynet & Maeder (2002), for instance.

In this regard, it seems pertinent to recall that our consideration of the  $(M_{F275W} - M_{F336W})_0$  colours of the the anomalous population of giants revealed that these stars are O-rich, which probably means that they have  $[O/Fe]$  values that are close to the maximum value (i.e.,  $[O/Fe] = 0.6$ ) since their UV colours overlap with those of normal giants (see Fig. 9). Unfortunately, it is not possible at this time to investigate the dependence of  $(M_{F275W} - M_{F336W})_0$  colours on the O abundance, as we do not have the capability to predict BCs for the  $F275W$  filter. Still, it is an intriguing possibility that the stars with apparently very low N and high O abundances may have formed out of gas that was not “contaminated” by the chemical evolution that occurred during the formation of GCs

(which produced the observed C–N–O–Na–Mg–Al–Si correlations and anticorrelations).

The  $(M_{F606W} - M_{F814W})_0$ ,  $M_{F606W}$  diagram remains something of a mystery as our models fail to explain the observed colour spreads along the lower RGB at a given magnitude. Since the  $F606W$  and  $F814W$  passbands are mostly sensitive to CN (see Sbordone et al. 2011), our failure could simply be an indication that we have not considered sufficiently high N abundances and/or the optimum ratios of C:N to maximize predicted CN strengths. This needs to be investigated. However, we suspect that this may not be a viable solution at the lowest metallicities given the decrease in the abundances of both C and N with decreasing  $[Fe/H]$  and the concomitant rapid decrease in CN strengths. Allowing for larger He abundance variations may help to resolve this problem, as would higher  $[CNO/Fe]$ , which would tend to reduce the separation in colour between the turnoff and the lower RGB. We doubt that the discrepancies between the predicted and observed colours are due mostly to errors in the model  $T_{\text{eff}}$  scale because, for the most part, our isochrones provide reasonable fits to the other CMDs that we have considered without having to apply temperature corrections.

Knowing the total C+N+O abundance in GCs is exceedingly important for fits of isochrones to observed CMDs (notably to the difference in colour between the TO and lower RGB) and for their ages. The evidence from binary stars seems compelling that  $[CNO/Fe] \gtrsim 0.44$ , which is obtained for a primordial mixture with  $[C/Fe] = [N/Fe] = 0.0$  and  $[O/Fe] = 0.6$ . Stellar models that assume  $[O/Fe] = [\alpha/Fe] = 0.4$  are precluded, not only by the binaries but also by the the high N abundances that are typically derived for cluster giants. For instance, if nearly all of the C and O in the high oxygen primordial mixture were converted to N via the CNO-cycle, the resultant N abundance would be close to  $[N/Fe] = 1.5$ , which is generally found in the majority of GCs (see, e.g., Cohen et al. 2002, Briley et al. 2004, Smith et al. 2005). Note that if the maximum values of  $[N/Fe]$  were closer to +1.7 (for which there is some spectroscopic support, see Briley et al. 2004, Cohen et al. 2005), such high abundances by themselves (i.e., without any contribution from C and O) would imply  $[CNO/Fe] = 0.65$ , which is 0.2 dex higher than we have assumed in the majority of our computations. Any increase in  $[CNO/Fe]$  would necessarily result in reduced ages at a given TO luminosity; consequently, the ages of  $\lesssim 12.8$  Gyr that we have obtained in this study using isochrones for  $[CNO/Fe] = 0.45$ , on the assumption of well-supported distances and reddenings, may be upper limits to their actual ages.

Although our stellar models appear to be able to reproduce the observed colours of GC stars and the widths of photometric sequences in cluster CMDs quite well, that success can be claimed only if the inferred abundances of C, N, and O from the superposition of the isochrones onto observed CMDs agree with the observed abundances. To answer such questions as “Do GC giants with the reddest  $(M_{F438W} - M_{F606W})_0$  colours have  $[C/Fe] \sim +0.5?$ ”, as implied by our isochrones, it is important to check such predictions spectroscopically. This is necessary because the model  $T_{\text{eff}}$  and hence colour scales are subject to many uncertainties (such as the treatment of convection and the atmospheric boundary condition). In fact, spectroscopic studies of member stars with the reddest and bluest  $(M_{F336W} - M_{F438W})_0$ ,  $(M_{F438W} - M_{F606W})_0$ , and  $(M_{F606W} - M_{F814W})_0$  colours are needed to validate the models. These samples should consist of isolated stars with the best possible photometry so that the colour spreads at a given magnitude can be defined to very high accuracy. Ideally, for consistency reasons, the spectroscopic analyses should employ the same MARCS model atmospheres and synthetic spectra that we have used, and

they should adopt temperatures and gravities very similar to those given by the stellar models. As we have emphasized throughout this study, comparisons of predicted and observed variations in colour at a given absolute magnitude should be more trustworthy than fits to the colours of individual stars.

A related issue that warrants some thought is whether the inferred abundances would be very different had we employed BCs based on 3D, instead of 1D, model atmospheres. It is well known that the strengths of molecular features are quite sensitive to 3D effects, mainly because of differences in the temperature structures of the outer atmospheres (see, e.g., Collet et al. 2006, Hayek et al. 2011, Amarsi et al. 2019a). Because the outer layers are cooler in 3D atmospheres of metal-poor stars, observed line strengths can be reproduced on the assumption of lower abundances of the metals (at fixed  $T_{\text{eff}}$ ,  $\log g$ , and  $[\text{Fe}/\text{H}]$ ) than in the case of 1D models. For instance, Hayek et al. (see their Figs. 18, 19) have found from their study of 3D models of the atmospheres of giants with  $\log g = 2.2$  that fits to CH, NH, and OH spectral features in the UV result in negative abundance corrections for C, N, and O, respectively — ranging up to as much as several tenths of a dex, with larger corrections occurring at the lower  $[\text{Fe}/\text{H}]$  values.

However, the extent to which such findings apply to the chemical abundances inferred here is not clear. The use of 3D atmospheres as boundary conditions for stellar interior models is bound to have some effect on the predicted  $T_{\text{eff}}$  scale, which is not constrained by empirical determinations to better than  $\sim \pm 70\text{--}100$  K; see, e.g., the compilation of temperatures and their uncertainties for the sample of dwarfs and giants given by Casagrande et al. 2010). Moreover, Chiavassa et al. (2018) have shown that BCs for broadband filters in the UV are affected at the level of up to a few hundredths of a magnitude, though the differences are much smaller for optical and IR passbands. Still, this is an important issue that should be investigated in due course.

The encouraging success that we have had in explaining the photometric properties of stellar populations in GCs with different abundances of C, N, and O gives us some optimism that our models will provide improved interpretations of chromosome maps. However, before applying our models to such maps, it will be necessary to extend the MARCS spectra further into the UV so that BCs for the  $F275W$  filter can be generated (and subsequently tested), and to produce model atmospheres, synthetic spectra, BCs, and stellar models for wider ranges in the nitrogen abundance as well as for additional C:N:O ratios to sample the observed C–N and O–N anticorrelations in more detail. Once the additional models are in hand, it should be possible to place reasonably tight constraints on the absolute light element abundances of stars in the most populous stellar populations and sub-populations that have been identified in GCs.

## ACKNOWLEDGEMENTS

We thank Kjell Eriksson for investigating the interplay between model atmospheres and synthetic spectra, Poul Erik Nissen and Anish Amarsi for valuable comments and suggestions after reading the initial version of this paper, and Karsten Brogaard, Pavel Denisenkov, John Norris, Peter Stetson, and David Yong for helpful information on various aspects of this project and for mentioning a few papers that we had overlooked. LC is the recipient of the ARC Future Fellowship FT160100402.

## DATA AVAILABILITY

Reference should be made to Paper I for information on how to obtain a selection of isochrones for  $[\text{Fe}/\text{H}] = -0.5, -1.5,$  and  $-2.5$  and all of the metal abundance mixtures that have been considered in this project, along with the means to transpose them from the theoretical H-R diagram to various CMDs. Grids of evolutionary tracks for finer spacings of  $[\text{Fe}/\text{H}]$ , assuming two or more helium abundances at each metallicity, are in the process of being computed; they will be made available to interested users once a separate paper describing these models has been submitted for publication.

## REFERENCES

- Amarsi, A. M., Nissen, P. E., Asplund, A., Lind, K., & Barklem, P. S. 2019a, *A&A*, 622, L4
- Amarsi, A. M., Nissen, P. E., & Skúladóttir, Á. 2019b, *A&A*, 630, A104
- Asplund, M., Grevesse, N., Sauval, A. J., & Scott, P. 2009, *ARAA*, 47, 481
- Baumgardt, H., & Vasiliev, E. 2021, *MNRAS*, 505, 5957
- Bedin, L. R., Piotto, G., Anderson, J., Cassisi, S., King, I. R., Momany, Y., & Carraro, G. 2004, *ApJ*, 605, L125
- Bellini, A., Bedin, L. R., Piotto, G., et al. 2010, *AJ*, 140, 631
- Bellini, A., Milone, A. P., Anderson, J., et al. 2017, *ApJ*, 844, 164
- Bergbusch, P. A., & Stetson, P. B. 2009, *AJ*, 138, 1455
- Briley, M. M., Cohen, J. G., & Stetson, P. B. 2004, *AJ*, 127, 1579
- Briley, M. M., Harbeck, D., Smith, G. H., & Grebel, E. K. 2004, *AJ*, 127, 1588
- Brogaard, K., VandenBerg, D. A., Bedin, L. R., Milone, A. P., Thygesen, A., & Grundahl, F. 2017, *MNRAS*, 468, 645
- Cannon, R. D., Croke, B. F. W., Bell, R. A., Hesser, J. E., & Stathakis, R. A. 1998, *MNRAS*, 298, 601
- Carbon, D., Barbuy, B., Kraft, R. P., Friel, E., & Suntzeff, N. B. 1987, *PASP*, 97, 335
- Carretta, E., Bragaglia, A., Gratton, R. G., D’Orazi, V., & Lucatello, S. 2009a, *A&A*, 508, 695 (CBG09)
- Carretta, E., Bragaglia, A., Gratton, R. G., & Lucatello, S. 2009a, *A&A*, 505, 139
- Carretta, E., Gratton, R. G., Lucatello, S., Bragaglia, A., & Bonifacio, P. 2005, *A&A*, 433, 597
- Carretta, E., Gratton, R. G., Bragaglia, A., Bonifacio, P., & Pasquini, L. 2004, *A&A*, 416, 925
- Casagrande, L., Ramírez, I., Meléndez, J., Bessell, M., & Asplund, M. 2010, *A&A*, 512, 54
- Casagrande, L., & VandenBerg, D. A. 2014, *MNRAS*, 444, 392 (CV14)
- Cassisi, S., Mucciarelli, A., Pietrinferni, A., Salaris, M., & Ferguson, J. W. 2013, *A&A*, 544, A19
- Chen, S., Richer, H., Caiazzo, I., & Heyl, J. 2018, *ApJ*, 867, 132
- Chiavassa, A., Casagrande, L., Collet, R., Magic, Z., Bigot, L., Thévenin, F., & Asplund, M. 2018, *A&A*, 611, A11
- Cohen, J. G., Briley, M. M., & Stetson, P. B. 2002, *AJ*, 123, 2525
- Cohen, J. G., Briley, M. M., & Stetson, P. B. 2005, *AJ*, 130, 1117
- Cohen, J. G., & Meléndez, J. 2005, *AJ*, 129, 303
- Collet, R., Asplund, A., & Trampedach, R. 2006, *ApJ*, 644, L121
- Correnti, M., Gennaro, M., Kalirai, J. S., Brown, T. M., & Calamida, A. 2016, *ApJ*, 823, 18
- Cybur, R. H., Fields, B. D., Olive, K. A., & Tsung-Han, Y. 2016, *RvMP*, 88, 015004
- Denissenkov, P. A., VandenBerg, D. A., Kopacki, G., & Ferguson, J. W. 2017, *ApJ*, 849, 159

- Dotter, A., Chaboyer, B., Jevremović, D., Kostov, V., Baron, E., Ferguson, J. W. 2008, *ApJS*, 178, 89
- Edvardsson, B., Andersen, J., Gustafsson, B., Lambert, D. L., Nissen, P. E., & Tomkin, J. 1993, *A&A*, 275, 191
- Fabbian, D., Nissen, P. E., Asplund, M., Pettini, M., & Akerman, C. 2009, *A&A*, 500, 1143
- Ferguson, J. W., & Dotter, A. 2008, in *IAU Symp. 252, The Art of Modeling Stars in the 21<sup>st</sup> Century*, ed. L. Deng, & K. I. Chan (Cambridge: Cambridge Univ. Press), 1
- Freeman, K. C., & Norris, J. 1981, *ARA&A*, 19, 319
- Fuhrmann, K. 2008, *MNRAS*, 384, 173
- Girardi, L., Castelli, F., Bertelli, G., & Nasi, E. 2007, *A&A*, 468, 657
- Gratton, R., Sneden, C., & Carretta, E. 2004, *ARA&A*, 42, 385
- Grevesse, N., Asplund, M., & Sauval, A. J. 2007, *SSRv*, 130, 105
- Grevesse, N., & Sauval, A. J. 1998, *SSRv*, 85, 161
- Grundahl, F., VandenBerg, D. A., & Andersen, M. I. 1998, *ApJ*, 500, L179
- Gustafsson, B., Edvardsson, B., Eriksson, K., Jorgensen, U. G., Nordlund, Å., & Plez, B. 2008, *A&A*, 486, 951
- Harris, W. E. 1996, *AJ*, 112, 1487
- Hayek, W., Asplund, M., Collet, R., & Nordlund, Å. 2011, *A&A*, 529, A158
- Ivans, I. I., Sneden, C., Kraft, R. P., et al. 1999, *AJ*, 118, 1273
- Johnson, C. I., McDonald, I., Pilachowski, C. A., et al. 2015, *AJ*, 149, 71
- Kaluzny, J. A., Thompson, I. B., Dotter, A., et al. 2014, *AcA*, 64, 11
- Kaluzny, J. A., Thompson, I. B., Dotter, A., et al. 2015, *AJ*, 150, 155
- King, I. R., Bedin, L. R., Cassisi, S., et al. 2012, *AJ*, 144, 5
- King, J. R., Stephens, A., Boesgaard, A. M., & Deliyannis, C. 1998, *AJ*, 115, 666
- Kraft, R. P. 1994, *PASP*, 106, 553
- Kraft, R. P., & Ivans, I. I. 2003, *PASP*, 115, 143
- Kurucz, R. L. 2005, *Mem.Soc.Astron.Ital.Suppl.*, 8, 76
- Kurucz, R. L. 2014, In “*Determination of the Atmospheric Parameters of B-, A-, F-, and G-Type Stars.*”, eds. E. Niemczura, B. Smalley, & W. Pych (Springer Cham), 39
- Laird, J. B. 1985, *ApJ*, 289, 556
- Marino, A. F., Milone, A. P., Piotto, G., et al. 2012a, *ApJ* 746, 14
- Marino, A. F., Milone, A. P., Sneden, C., et al. 2012b, *A&A*, 541, A15
- Marino, A. F., Milone, A., Sills, A., et al. 2019, *ApJ*, 887, 91
- Martins, F., Chantreau, W., & Charbonnel, C. 2017, *SF2A: Proc. Annual Meeting of the French Society of Astronomy & Astrophysics*, eds. C. Reylé, P. D. Matteo, F. Herpin, E. Langade, A. Lançon, Z. Meliani, & F. Royer, 57
- Meynet, G., & Maeder, A. 2002, *A&A*, 390, 561
- Milone, A., Marino, A. F., Piotto, G., et al. 2012, *ApJ*, 745, 27
- Milone, A., Marino, A. F., Piotto, G., et al. 2013, *ApJ*, 745, 27
- Milone, A. P., Marino, A. F., Piotto, G., et al. 2015a, *ApJ*, 808, 51
- Milone, A. P., Marino, A. F., Piotto, G., et al. 2015b, *MNRAS*, 447, 927
- Milone, A. P., Marino, A., Renzini, A., et al. 2018, *MNRAS*, 481, 5098
- Milone, A. P., Marino, A. F., Renzini, A., et al. 2020, *MNRAS*, 497, 3846
- Milone, A., Piotto, G., Bedin, L. R., et al. 2012, *ApJ*, 744, 58
- Milone, A. P., Piotto, G., King, I. R., et al. 2010, *ApJ*, 709, 1183
- Milone, A., Piotto, G., Renzini, A., et al. 2017, *MNRAS*, 464, 3636
- Nardiello, D., Libralato, M., Piotto, G., et al. 2018, *MNRAS*, 481, 3382 (NLP18)
- Nardiello, D., Piotto, G., Milone, A. P., et al. 2015, *MNRAS*, 451, 312
- Nissen, P. E., Chen, Y. Q., Carigi, L., Schuster, W. J. & Zhao, G. 2014, *A&A*, 568, A25
- Pietrinferni, A., Cassisi, S., Salaris, M., Percival, S., & Ferguson, J. W. 2009, *ApJ*, 697, 275
- Piotto, G., Bedin, L. R., Anderson, J., et al. 2007, *ApJ*, 661, L53
- Piotto, G., Milone, A. P., Bedin, L. R., et al. 2015, *AJ*, 149, 91
- Ramírez, I., Allende Prieto, C., & Lambert, D. L. 2013, *ApJ*, 764, 78
- Roederer, I. U., & Sneden, C. 2011, *AJ*, 142, 22
- Salaris, M., Weiss, A., Ferguson, J. W., & Fusilier, D. J. 2006, *ApJ*, 645, 1131
- Saracino, S., Dalessandro, E., Ferraro, F. R., et al. 2018, *ApJ*, 860, 95
- Sbordone, L., Salaris, M., Weiss, A., & Cassisi, S. 2011, *A&A*, 534, A9
- Schlafly, E. F., & Finkbeiner, D. P. 2011, *ApJ*, 737, 103
- Schlegel, D., Finkbeiner, D. P., & Davis, M. 1998, *ApJ*, 500, 525
- Shetrone, M. D. 1996, *AJ*, 112, 2639
- Smith, G. H. 1987, *PASP*, 99, 67
- Smith, G. H., Briley, M. M., & Harbeck, D. 2005, *AJ*, 129, 1589
- Smith, G. H., & Norris, J. E. 1993, *AJ*, 105, 173
- Smith, G. H., Shetrone, M. D., Bell, R. A., Churchill, C. W., & Briley, M. M. 1996, *AJ*, 112, 1511
- Sneden, C., Kraft, R. P., Guhathakurta, P., Peterson, R. C., & Fulbright, J. P. 2004, *AJ*, 127, 216
- Spite, M., Cayrel, R., Plez, B., et al. 2005, *A&A*, 430, 655
- Thompson, I. B., Udalski, A., Dotter, A., et al. 2020, *MNRAS*, 492, 4254
- Tomkin, J., & Lambert, D. L. 1984, *ApJ*, 279, 220
- VandenBerg, D. A., Bergbusch, P. A., Dotter, A., Ferguson, J. W., Michaud, G., Richer, J., & Proffitt, C. R. 2012, *ApJ*, 755, 15
- VandenBerg, D. A., Bergbusch, P. A., Ferguson, J. W., & Edvardsson, B. 2014a, *ApJ*, 794, 72
- VandenBerg, D. A., Brogaard, K., Leaman, R., & Casagrande, L. 2013, *ApJ*, 775, 134 (VBLC13)
- VandenBerg, D. A., Casagrande, L., & Stetson, P. B. 2010, *AJ*, 140, 1020
- VandenBerg, D. A., & Denissenkov, P. A. 2018, *ApJ*, 862, 72
- VandenBerg, D. A., Denissenkov, P. A., & Catelan, M. 2016, *ApJ*, 827, 2
- VandenBerg, D. A., Edvardsson, B., Casagrande, L., & Ferguson, J. W. 2021, *MNRAS*, in press (Paper I)
- Van Eck, S., Neyskens, P., Jorissen, A., et al. 2017, *A&A*, 601, A10
- Wylie, E. C., Cottrell, P. L., Sneden, C. A., & Lattanzio, J. C. 2006, *ApJ*, 649, 248
- Yong, D., Grundahl, F., D’Antona, F., Karakas, A. I., Lattanzio, J. C., & Norris, J. E. 2009, *ApJ*, 695, L62
- Yong, D., Grundahl, F., Nissen, P. E., Jensen, H. R., & Lambert, D. L. 2005, *A&A*, 438, 875
- Yong, E., Aoki, W., & Lambert, D. L. 2006, *ApJ*, 638, 1018